Implementation of the PCGP Algorithm for Characterization of XUV Laser Pulses

Master's thesis
by
Thomas Lennartsson

Lund Reports on Atomic Physics, LRAP-346
Lund, August 2005

Abstract

In this work an algorithm for characterization of ultrashort laser pulses in the XUV region has been developed. Measurement data are obtained by the method of Frequency Resolved Optical Gating (FROG), which is based on spectrally resolving the signal received from two pulses overlapping with each other in an autocorrelation experiment. The experimental data – the FROG trace – is then used as the input in an algorithm based on the method of Principal Component Generalized Projections (PCGP); the output is both envelope and phase of the two pulses. The algorithm has been tested on both simulated and real FROG traces. These traces have either been high-order harmonics of femtosecond duration or attosecond pulse trains. The results of these tests are promising, showing that FROG techniques combined with the PCGP algorithm is a reliable method for characterizing ultrashort laser pulses.

Contents

Chapter 1

Introduction

One of the major scientific breakthroughs during the last century was the invention of the laser in 1960. Ever since, the laser has given rise to a number of applications which have had a tremendous impact on both science and society in general. Lasers generate light with properties superior to that of other radiative sources, be it in terms of coherence as well as intensity.

A significant part of the technological development has been focused on the generation of shorter and shorter pulses of laser light. Today, the achievements in this area of physics have pushed the lower limit of duration to a few femtoseconds (fs, 10^{-15} seconds) for pulses in the visible and near-infrared region. Using wavelengths in the extreme ultraviolet (XUV) to soft X-ray regime the femtobarrier has recently been broken, allowing physicists to enter the attosecond (as, 10^{-18} seconds) area of ultrashort laser technology. The struggle to achieve shorter and shorter pulses has mainly two reasons. First, these pulses enable precise measurements of ultrafast phenomena. The development of the femtosecond laser has for example provided chemists with a tool of incredible temporal resolution, which has given rise to a new scientific branch known as femtochemistry. In atoms, electrons move around the atomic nucleus on the attosecond scale, and the newly generated and measured attosecond pulses will hopefully be used to probe the motion. Second, with shorter pulses, higher peak power can be achieved. This enables high intensity physics at relatively low pulse energies.

When pushing the limits of pulse duration, it is also necessary to be able to characterize the pulses one manages to produce. When entering the femtosecond regime and below, pulse characterization becomes somewhat problematic, which is due to the fact that the response time of electronic devices can be pushed down to the picosecond (ps, 10^{-12} seconds) regime, but no further. Other than that, the pulses produced in laboratories might be of frequencies in the XUV regime or of shorter wavelengths. This introduces further difficulties, since suitable optical components are hard to find in that part of the spectrum. Intricate methods for pulse characterization are therefore needed, and have been

developed during the past years. This diploma project has been focused on one of these methods: Frequency-Resolved Optical Gating (FROG) [1]. Its primary concern has been to construct an algorithm which succeeds in reconstructing ultrashort pulses from measured FROG data, and especially those obtained in the XUV range corresponding to harmonic radiation of femtosecond and even attosecond duration.

This thesis will begin with a short summary of the behaviour of ultrashort laser pulses in general in chaper 2, focusing on the generation and characteristics of harmonic XUV radiation. Chapter 3 will describe the FROG technique in detail. The algorithm for pulse characterization will be reviewed in Chapter 4, and finally, results connected to characterization experiments will be presented in Chapter 5.

Chapter 2

Description and Generation of Short Light Pulses

Before trying to develop a technique for measuring ultrashort laser pulses, one obviously needs to know the basic theories of these pulses. Therefore this chapter will give a brief introduction on the mathematical description of ultrashort laser radiation, where important terms such as 'chirp' and the time-bandwidth product will be explained. Further into the chapter, the theories of harmonic XUV radiation and the basic characteristics of such pulses will be discussed.

2.1 Description of Short Pulses

This section will concern the mathematical description of short laser pulses. The complex representation of the electric field will be presented, as well as both temporal and spectral aspects of the field. The importance of the phase of the pulse and its temporal behaviour will also be discussed.

2.1.1 Complex Representation of the Electric Field

Even though the measured quantities which originate from the electric field $\vec{E}(\vec{r},t)$ are real, it might often be convenient to represent the field itself in a complex form. Since this project mainly focuses on the temporal properties of the field, its spatial dependence will throughout this thesis be neglected; that is $\vec{E}(\vec{r},t) = E(t)$.

We now define the complex spectrum of $E(t)$ as the Fourier transform of the electric field [2]:

$$\tilde{E}(\omega) = \mathcal{F}\left[E(t)\right] = \int_{-\infty}^{+\infty} E(t) \cdot e^{-i\omega t} dt = |\tilde{E}(\omega)| \cdot e^{i\Phi(\omega)} \tag{2.1}$$

Here the tilde is used to denote the Fourier transform as a complex parameter. $|\tilde{E}(\omega)|$ is the spectral amplitude, and $\Phi(\omega)$ is the phase of the spectrum. From $\tilde{E}(\omega)$ we can reconstruct $E(t)$ by applying the inverse Fourier transform:

$$E(t) = \mathcal{F}^{-1}\left[\tilde{E}(\omega)\right] = \frac{1}{2\pi}\int_{-\infty}^{+\infty} \tilde{E}(\omega)\cdot e^{i\omega t}d\omega \tag{2.2}$$

The Fourier transform of the electric field can be interpreted as a way of describing the frequency content of the field, or – correspondingly – its energy content. From equation 2.2 one can see that every electric field $E(t)$ can be considered as being a superposition of plane waves. Since negative frequencies in this context don't have any physical relevance, one would like a more suitable way of representing the field. This can be done with the introduction of the complex electric field:

$$\tilde{E}^{+}(t) = \frac{1}{2\pi}\int_{0}^{+\infty} \tilde{E}(\omega)\cdot e^{i\omega t}d\omega \tag{2.3}$$

Now the spectrum of this complex field can be written as:

$$\tilde{E}^{+}(\omega) = \int_{-\infty}^{+\infty} \tilde{E}^{+}(t)\cdot e^{-i\omega t}dt = \begin{cases} |\tilde{E}(\omega)|\cdot e^{i\Phi(\omega)} & \omega \geq 0 \\ 0 & \omega < 0 \end{cases} \tag{2.4}$$

The real electric field can be expressed by the sum

$$E(t) = \tilde{E}^{+}(t) + \tilde{E}^{-}(t) \tag{2.5}$$

where $\tilde{E}^{-}(t)$ is for the negative frequencies what $\tilde{E}^{+}(t)$ is for the positive. The complex field can also be expressed as

$$\tilde{E}^{+}(t) = A(t)\cdot e^{i\Gamma(t)} \tag{2.6}$$

where $A(t)$ is an amplitude function, and $e^{i\Gamma(t)}$ is a phase term. From Poynting's theorem [3] we can now deduce that the intensity of the electric field $I(t)$ is proportional to $|\tilde{E}^{+}(t)|^2$. The quantity which is being measured with a spectrometer $S(\omega)$ is called the spectral intensity and is found to be proportional to $|\tilde{E}^{+}(\omega)|^2$.

From now on, a more simple notation will be used: we drop the tilde and the plus sign; $E(t)$ represents the complex electric field and $E(\omega)$ refers to the complex spectrum of $E(t)$. Note that these two notations are refering to two different functions, and not just a change in variable denotation.

2.1.2 The Phase Function

A short laser pulse is often described by the form of equation 2.6. $A(t)$ describes the temporal profile of the pulse – its envelope. In passively mode-locked laser systems, the theoretical pulse shape is a sech function; in actively mode-locked systems the generated pulses are Gaussian. The shape may however in principle be of another more complex form.

In most cases the spectrum of the field will be centered around a mean (angular) frequency ω_0, and the width of the spectrum will be small compared to this central frequency. $\Gamma(t)$ will therefore be expanded as follows:

$$\Gamma(t) = \omega_0 t + \Phi(t) \tag{2.7}$$

$\Phi(t)$ is called the (temporal) phase and may or may not be time dependent. To understand what is the influence of this phase on the electric field, we express the instantaneous angular frequency as [2]:

$$\omega(t) = \frac{d\Gamma(t)}{dt} = \omega_0 + \frac{d\Phi(t)}{dt} \tag{2.8}$$

If $\Phi(t)$ is just an arbitrary constant, the frequency of the pulse will not be affected. If the phase is linearly dependent of t, a constant frequency shift will be introduced to the spectrum and the expansion of $\Gamma(t)$ will not be unique. With the introduction of a higher order dependence of $\Phi(t)$, the instantaneous frequency will be varied with time – the pulse is said to be 'chirped'. If $\frac{d^2\phi(t)}{d^2t} < 0$, the frequency decreases with time and the pulse is said to be negatively chirped, and if the opposite applies, the frequency increases – the chirp is positive.

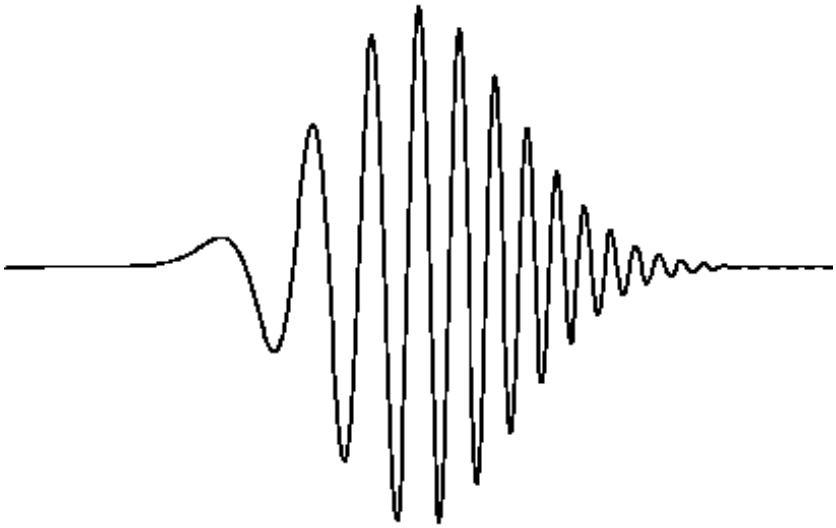

Figure 2.1: The electric field of a positively chirped pulse, as a function of time. Note how the frequency of the pulse increases with time.

2.1.3 Pulse Duration and Bandwidth

In order to examine the correspondance between the temporal and the spectral domain, we will now study a pulse with a Gaussian envelope. The reason for this is the fact that the Fourier transform of a Gaussian function also is Gaussian, and the problem becomes therefore relatively easy to handle. We can in general write the electric field of a Gaussian pulse as:

$$E(t) = e^{-at^2} \cdot e^{i(\omega_0 t + \frac{b}{2}t^2)} \tag{2.9}$$

The electric field of the pulse exhibits in this case a quadratic phase behaviour, controlled by the parameter $b/2$. The frequency will therefore vary linearly with time as bt. The parameter a is used to define the width of the pulse and is related to the full width at half maximum (FWHM) $\Delta\tau$ by:

$$a = \frac{2\ln 2}{(\Delta\tau)^2} \tag{2.10}$$

Ignoring a scaling constant as well as a constant phase term, the complex spectrum of the Gaussian pulse becomes [4]:

$$E(\omega) = e^{-\frac{(\omega-\omega_0)^2}{4(a-ib/2)}} = e^{-\frac{a(\omega-\omega_0)^2}{4(a^2+(b/2)^2)}} \cdot e^{-i\frac{b(\omega-\omega_0)^2}{8(a^2+(b/2)^2)}} \tag{2.11}$$

From this expression one can instantly make two conclusions: First, a quadratic temporal phase also gives rise to a quadratic dependency of the spectral phase; second, the width of the frequency distribution is both dependent on the duration of the pulse as well as on the chirp. The bandwidth $\Delta\omega$ is defined as the FWHM of the spectral distribution:

$$\Delta\omega = \sqrt{8\ln 2}\sqrt{a(1+\frac{b^2}{4a^2})} \tag{2.12}$$

From this expression it is seen that for a given pulse duration, the presence of a linear chirp requires a broader bandwidth. Correspondingly, for a given spectral width, a linear chirp causes the pulse to spread out more in time.

By multiplying equation 2.10 with expression 2.12, one obtains the so called time-bandwidth product:

$$\Delta\omega\Delta\tau = 2\pi \cdot 0.441 \cdot \sqrt{1+\frac{b^2}{4a^2}} \geq 2\pi \cdot 0.441 \tag{2.13}$$

One can see that there is a minimum value for this product. When equality in equation 2.13 holds, the pulse is the shortest possible, given the spectral bandwidth. This occurs when the pulse exhibits no frequency chirp, and it is then said to be Fourier limited.

The properties of the time-bandwidth product holds for all pulse shapes [2], and can be written in a more general form as:

$$\Delta\omega\Delta\tau \geq 2\pi c_B \tag{2.14}$$

The value of c_B will be different depending on which pulse structure the product refers to. When comparing equation 2.14 with equation 2.13, one identifies the value of c_B as being 0.441 for a Gaussian pulse, while the corresponding value is 0.315 when considering the hyperbolic secant envelope [5].

2.2 High-Order Harmonics

High-order harmonic generation (HHG) is a nonlinear process taking place when a strong laser field interacts with atoms, for instance rare gases. Since the intensities needed for the process to occur are very high, only lasers which are able

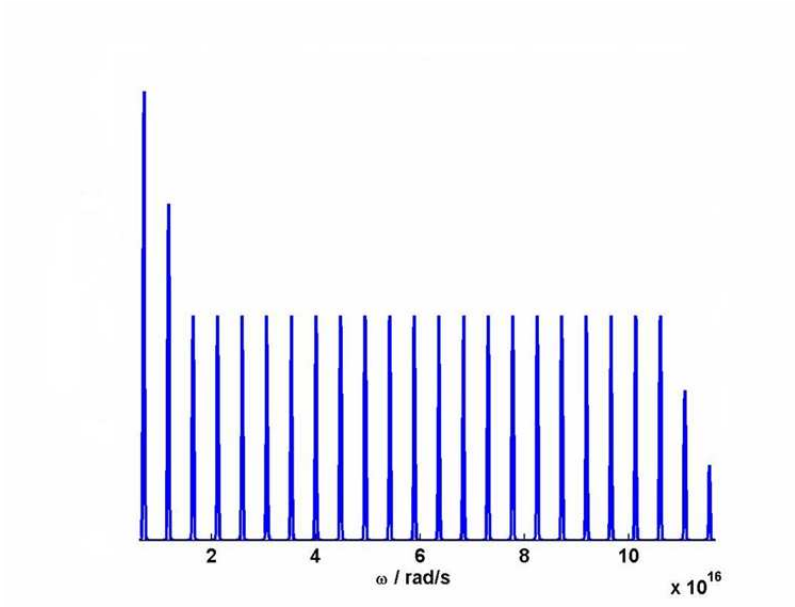

Figure 2.2: Plateau of high-order harmonics, extending from the UV into the soft X-ray regime. In the beginning of the spectrum are the low-order harmonics, and at the far end, the frequency comb experiences a sudden cut-off.

to produce pulses with very short duration can be used to study this phenomenon. Due to the technique of short pulse generation by mode-locking, HHG was observed for the first time in 1987, and in the early 1990's, chirped pulse amplification made it possible to use table-top high-power lasers in order to routinely study the phenomenon.

The high harmonic radiation produced by an ultrashort, intense laser pulse consists of a frequency comb spanning a broad bandwidth [6], from the UV down to the soft X-ray region, as can be seen in figure 2.2. The first few peaks in the figure represents the low-order harmonics. Each tooth of the comb is an odd multiple of the frequency of the generating laser pulse, and is separated from its neighbours by twice this fundamental frequency. On the one hand, every tooth corresponds to a short femtosecond pulse of XUV radiation. On the other hand, due to the large bandwidth, HHG offers an opportunity to superimpose all the harmonics, thereby generating XUV bursts of attosecond duration.

2.2.1 Experimental Setup for High-Order Harmonic Generation

An outline of the setup for HHG at the Atomic Physics Division in Lund is shown in figure 2.3. An infrared (800 nm) beam of laser pulses enters the setup at a rate of 1 kHz. The pulses are focused into a gas, which usually is argon

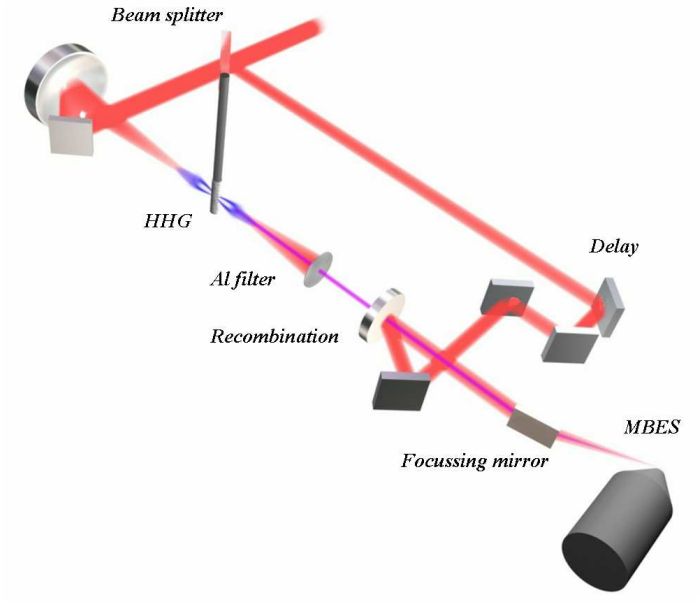

Figure 2.3: Experimental setup for high-order harmonic and attosecond pulse train generation. After the generation stage there is a final stage for characterization of the signal generated.

or neon, and is being pumped into the system in a tube with two small holes drilled by the laser, inserted into a vacuum chamber. When the intensity of the infrared beam is of the order of 10^{14}–10^{15} W/cm^2, high-order harmonics will be generated [6].

The next step in the setup is by spectally and spatially filtering the harmonics using these for attosecond pulse train generation. These pulses are thereafter in the final stage, being measured by cross-correlating with the initial beam of IR pulses. These stages will be more carefully explained further into this thesis.

2.2.2 The Three-Step Model

The rapid drop in amplitude of the first low-order harmonics (which is seen in figure 2.2) can be predicted by perturbation theory. This is however not the case for the high-order harmonics, with approximately constant amplitude over a large energy range. The intensity of the laser field is so strong that it no longer can be regarded as a small perturbation to the system. We can however give a simple picture of the underlying physics, based upon semi-classical considerations. This picture is the so called three-step model (TSM) [7], which is based on the assumption that it is possible for the electron wavepacket to tunnel out into the continuum, when the Coulomb potential of the atom is highly deformed by the field. The three steps are shown in figure 2.4, and are as follows:

1. Through quantum mechanical tunneling, the electron is moved into the

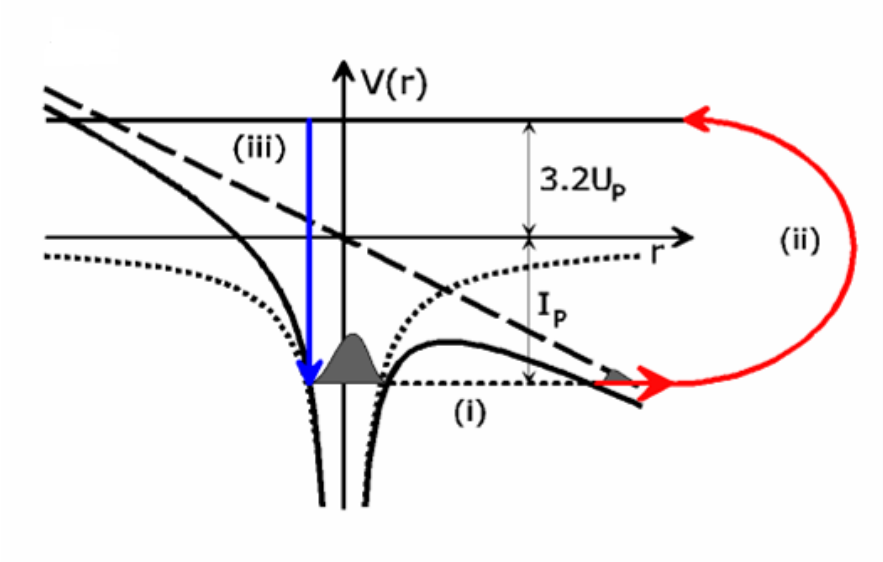

Figure 2.4: Visualisation of TSM: (i) The electron wavepacket tunnels through the deformed Coulomb potential of the atom, out into the continuum. (ii) It is accelerated in the continuum by the laser field. (iii) It returns to the atom, sending out its excess energy in the form of a photon.

continuum, with zero kinetic energy.

2. The electron is now regarded as a classical particle, and is accelerated by the external laser field, gaining kinetic energy.
3. Depending on the phase of the laser field at the time of release in the continuum, the electron may come back to the atom. Doing so, the energy gained in the continuum is released in the form of a high frequency photon – a high harmonic.

This high harmonic generation process is periodic with a period of $T_L/2$, where T_L is the period of the driving laser field. This leads to generation of harmonics whose frequencies are only odd multiples of the driving field. The harmonics will therefore, if the driving frequency is ω_0, be separated by a frequency of $2\omega_0$. The energy of each harmonic is dependent on the time the electron wave packet spends in the continuum, which in its turn is decided by the phase of the laser field at the time the electron tunnels out of the atomic potential. If the electron gets out before the field has reached its maximum ($\omega_0 t = \frac{\pi}{2}$), it will never recombine with the atom. Electrons which tunnel through at a later stage will however return to the atom, emitting high harmonic radiation. When the electron is released into the continuum at approximatly $\omega_0 t = 1.19 \cdot \frac{\pi}{2}$, it will gain the highest energy possible $W_{max} = 3.2U_p$, where U_p is defined as:

$$U_p = \frac{e^2 E^2}{4m\omega_0^2} \tag{2.15}$$

Here m is the mass of the electron in rest, and U_p, which is called the ponder-motive energy, is being interpreted as the average kinetic energy the electron

acquires in the continuum. Hence, the cut-off of the harmonic plateau occurs at the energy

$$W = I_p + 3.2U_p \tag{2.16}$$

where I_p is the ionisation energy of the atom.

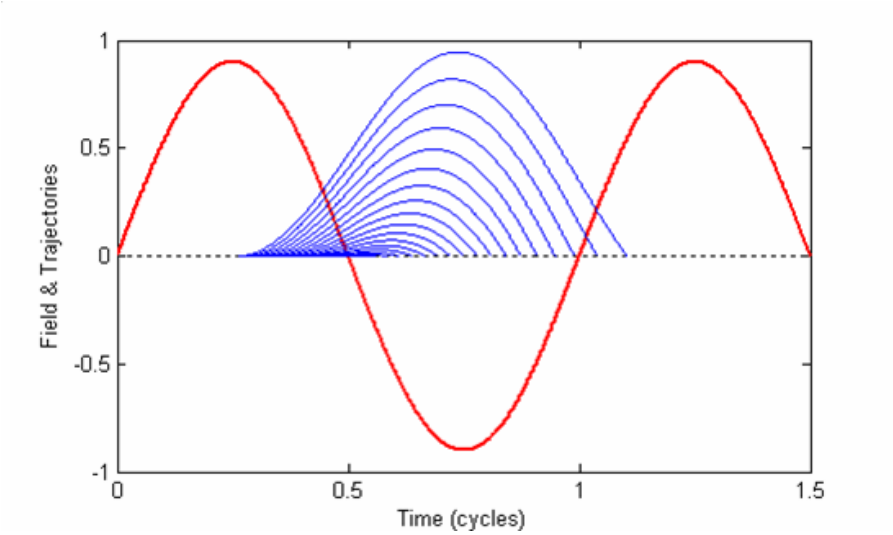

Figure 2.5: Red: The electric field of the fundamental laser field. Blue: Electron trajectories originating from tunnel ionisation due to the fundamental field.

The electron while accelererated by the laser field, can be regarded as moving in the continuum along certain trajectories, as depicted in figure 2.5. Each trajectory is characterized by a certain return time for the electron. For every possible harmonic energy there are several different return times and trajectories, which is shown in figure 2.6. The first two are called the 'short' respectively the 'long' trajectory. This is valid for every return energy, except for the maximum energy, for which there is only one.

2.2.3 Time Dependent Schrödinger Equation Treatment of High-Order Harmonic Generation

While the TSM gives a good qualitative picture of the harmonic generation process, it is too approximative to give good quantitative predictions. A full quantum mechanical formulation of the problem is therefore desired. This is done by solving the time-dependent Schrödinger equation (TDSE) [7]. Two initial assumptions are made:

1. Only one electron contributes to the process. Any interaction terms between the electrons in the atom are therefore left out.
2. The intensity of the external laser field is very strong, which means that the photon density is very high. Hence, we can use a semi-classical approach, where the laser field is treated classically as a continuous quantity.

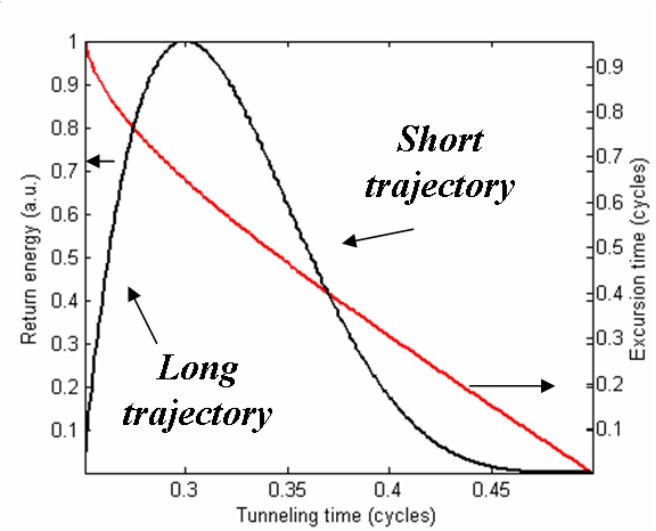

Figure 2.6: Return energy and excursion time for the returning electron as a function of time of tunneling.

The TDSE for this specific problem is then, in atomic units ($m = e = \hbar = 1$):

$$i\frac{\partial}{\partial t}|\Psi(\vec{r},t)\rangle = \left[-\frac{1}{2}\nabla^2 + V(\vec{r}) + W(\vec{r},t)\right]|\Psi(\vec{r},t)\rangle \tag{2.17}$$

Here $V(\vec{r})$ is the atomic potential, $W(\vec{r},t)$ is the term connected to the laser field and $\Psi(\vec{r},t)$ is the wave function for the electron. A number of approximations concerning the laser field is now being made: It is regarded as being uniform across the atom, i.e. the wavelength is much larger than the width of the atom; contributions from the magnetic dipole and electric quadrupoles are neglected; the laser field is linearly polarised in the x-direcetion. One can now write the laser field term as:

$$W(x,t) = -E_0\cos(\omega_0 t)x \tag{2.18}$$

From the solution of equation 2.17 one can calculate the induced dipole moment, which is related to the separation of the charges in the atom:

$$D(\vec{r},t) = \langle\Psi(\vec{r},t)|x|\Psi(\vec{r},t)\rangle \tag{2.19}$$

2.2.4 Strong Field Approximation

In order to perform the calculation of equation 2.19, one can apply the strong-field approximation [8]. The result is in the end a decomposition of the dipole moment, each term D_q corresponding to one specific harmonic frequency, $q\omega_0$, where q equals an odd integer:

$$D_q = \sum_j A_j^q \cdot e^{i\Phi_j^q} \tag{2.20}$$

The summation above is made over all different electron trajectories, labled j, corresponding to one given harmonic energy. In principle the number of trajectories is infinite, but in practice one can reduce the sum to just cover the first few. A_j^q represents the strength of each dipole component, and Φ_j^q each component's phase.

The radiation field $E_q(t)$ corresponding to each harmonic can now be calculated:

$$E_q(t) = D_q e^{iq\omega_0 t} = \sum_j A_j^q \cdot e^{i(q\omega_0 t + \Phi_j^q)} \tag{2.21}$$

2.2.5 Harmonic Chirp

When making harmonic pulses in the laboratory, one wants to make them as short as possible. Having the discussion in section 2.1.3 in mind, one thus has to suppress the chirp of the harmonics, or else the pulse – given a spectral bandwidth – will be broadened. Before one can minimize the harmonic chirp, one must however know its origin and characteristics, which is what will be discussed in the following paragraphs.

Given a specific harmonic order q and a given trajectory j, the phase of each harmonic component will be dependent on the intensity of the driving laser field [9]. The intensity dependence of the dipole phase leads to a chirp of the harmonic pulse. The harmonic is generated with a laser pulse for which the intensity varies in time, $I(t)$. This means that the dipole phase, and hence the phase of the harmonic generated also depends on time:

$$\Gamma(t) = q\omega_0 t + \alpha I(t) \tag{2.22}$$

The instantaneous frequency is now written as:

$$\omega(t) = q\omega_0 + \alpha \frac{\partial I(t)}{\partial t} \tag{2.23}$$

Comparing equation 2.23 with equation 2.8 one can identify α as $\alpha = \partial\Phi/\partial I$.

We now look at the linear chirp which is induced by the intensity dependence. $\Gamma(t)$ is now written as $\Gamma(t) = q\omega_0 t + b_l t^2/2$. The linear chirp rate b_l is then given by the second derivative of $\Gamma(t)$, which reduces to the second derivative of $\Phi(t)$. b_l can therefore be written as:

$$b_l = \frac{\partial^2 \Phi}{\partial t^2} = \frac{\partial}{\partial t}\left(\frac{\partial I}{\partial t} \cdot \frac{\partial \Phi}{\partial t}\right) = \frac{\partial \Phi}{\partial I}\frac{\partial^2 I}{\partial t^2} + \frac{\partial^2 \Phi}{\partial I^2}\left(\frac{\partial I}{\partial t}\right)^2 \tag{2.24}$$

One now assumes a Gaussian pulse envelope with the top intensity I_0 and the FWHM denoted as $\Delta\tau$. The first and second time derivatives can then be calculated as:

$$\frac{\partial I}{dt} = -\frac{8\ln 2}{(\Delta\tau)^2} I_0 t \cdot e^{-\frac{4\ln 2}{(\Delta\tau)^2}t^2} \tag{2.25}$$

$$\frac{\partial^2 I}{dt^2} = \left[-\frac{8\ln 2}{(\Delta\tau)^2} I_0 + \left(\frac{8\ln 2}{(\Delta\tau)^2} \right)^2 I_0 t^2 \right] \cdot e^{-\frac{4\ln 2}{(\Delta\tau)^2} t^2} \tag{2.26}$$

Assuming harmonics being generated at the top of the pulse, we can set $t = 0$ and by combining equation 2.24 with equations 2.26 and 2.25 we get:

$$b_l \approx -8\ln(2) \frac{I_0}{(\Delta\tau)^2} \frac{\partial\Phi}{\partial I} \tag{2.27}$$

For harmonics it is found that this so called harmonic chirp as good as always is negative. The magnitude of the chirp will increase with $\partial\Phi/\partial I$ and the peak laser intensity I_0. It is inversely proportional to the square of the fundamental pulse width $\Delta\tau$. Also, the harmonic chirp would be zero if the envelope of the fundamental was constant.

If the fundamental carries a chirp b_{fund}, it will be propagated in the generated harmonics as qb_{fund}. The total harmonic chirp b then becomes:

$$b = qb_{fund} + b_l = qb_{fund} - 8\ln(2) \frac{I_0}{(\Delta\tau)^2} \frac{\partial\Phi}{\partial I} \tag{2.28}$$

This means that while the first term in equation 2.28 might either be positive or negative, depending on the sign of the fundamental chirp, the second term almost always assumes negative values. Using this insight one could in principle construct a harmonic pulse without a chirp, through inducing a small positive chirp on the fundamental, compensating the chirp due do the harmonic generation process itself.

2.3 Attosecond Pulse Generation

The bandwidth of the high harmonic plateau makes it in principle possible to create pulses down to a few tens of attoseconds [10]. In order to successfully produce short attosecond pulses, optimisation of the amplitude and phase of the generated harmonics must be achieved. This section will discuss experimental aspects of attosecond pulse generation, as well as the phase behaviour needed for obtaining short attosecond pulses.

2.3.1 Experimental Setup

The basic setup for generation of attosecond pulse trains is shown in figure 2.3. After HHG, the harmonic radiation is made to propagate through an 600 nm-thick aluminium filter. The aluminium spectrally filters out all the radiation with frequencies lower than about the 13th harmonic order. By its group velocity dispersion, the filter also mode locks the harmonics transmitted. Harmonics originating from several trajectories are now constituting the radiation. This is not desireable, since there (as one can understand from figure 2.6) is a big phase difference between different trajectories. Fortunately, the radiation from the long trajectory is considerably more divergent than the radiation originating from the short trajectoy. By spatially filtering the light by making it to

propagate through a small hole, one thereby obtains harmonics only from the short trajectory, and the pulse duration is thereby reduced further.

2.3.2 Mathematical Description

Superimposing the high-order harmonics in a frequency comb, from the first q_i to the last q_f, and making use of equation 2.21, results in the electric field $E(t)$:

$$E(t) = \sum_{q=q_i}^{q_f} E_q(t) = \sum_{q=q_i}^{q_f} A_q \cdot e^{i(q\omega_0 t + \Phi_q)} \tag{2.29}$$

If $\Phi_q = 0$ and $q_i = 13$, $q_f = 19$, the intensity distribution obtained will have

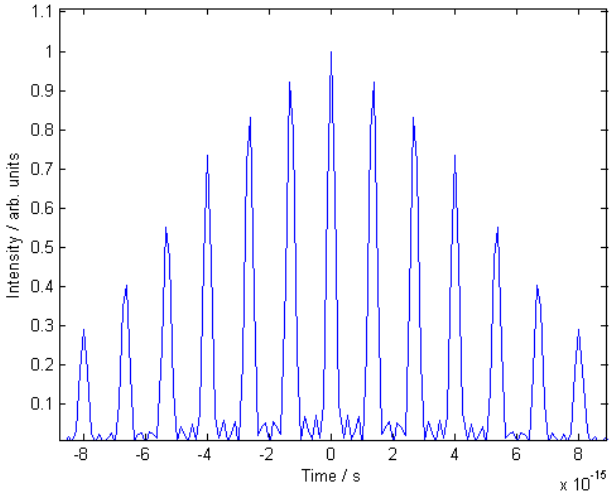

Figure 2.7: Attosecond pulse train arising from the superposition of harmonics 13 to 19.

the appearance of figure 2.7 – a train of pulses of a few hundreds attoseconds width, separated by half the fundamental laser period, and spanning over an interval of a few tens of femtoseconds.

2.3.3 Attosecond Chirp

Even if one manages to eliminate the harmonic chirp, Φ_q may still be equal to a function which is not equal to zero – the so called 'atto chirp' [9]. While the harmonic chirp is due to the intensity variation of the fundamental laser field, the atto chirp would be present even if the fundamental intensity was fixed. This is due to the fact that different harmonic orders correspond to different electron trajectories and thus different emission times. While the harmonic chirp is an intrinsic chirp of each harmonic, the atto chirp thus is the chirp *between* harmonics. The time scale of the two different kinds of chirp are thus different;

the atto chirp takes place within the time of one laser cycle, whereas the femto chirp is induced over the whole laser envelope. This may be depicted as is done in figure 2.8. Like the harmonic chirp may broaden the harmonic pulse, the atto chirp broadens the pulses in the attosecond train. It is thus important to surpress the atto chirp if intending to make as short pulses as possible.

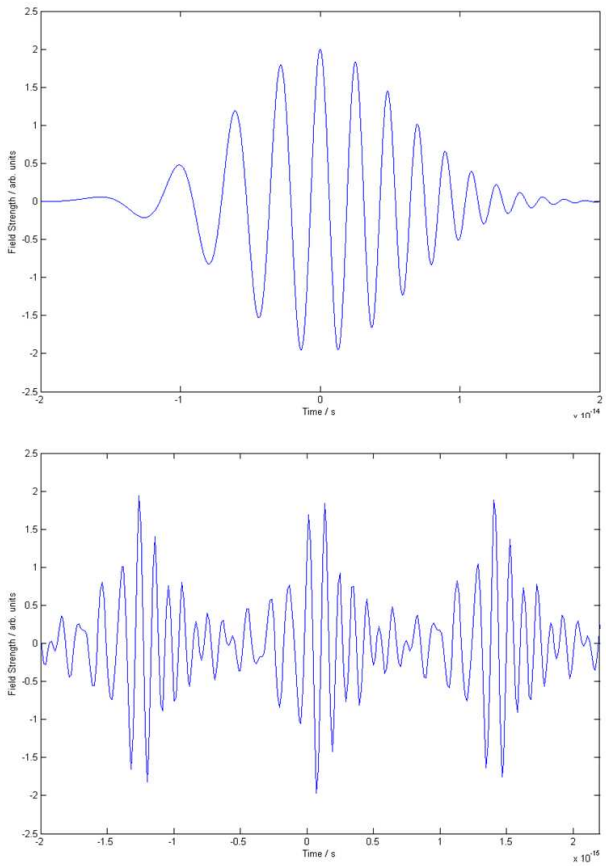

Figure 2.8: Above: Harmonic pulse in the femtosecond regime, exhibiting a phase modulation proportional to t^2, giving rise to a harmonic chirp. Below: Train of pulses in the attosecond regime, exhibiting a phase modulation proportional to q^2, giving rise to an atto chirp.

The discussion above can be expressed in a more mathematical way. Consider a linear dependence of the phase with respect to q, $\Phi_q = cq$. This will give rise to a pulse train on the form of:

$$E(t) = \sum_{q=q_i}^{q_f} A_q \cdot e^{i(q\omega_0 t + cq)} = \sum_{q=q_i}^{q_f} A_q \cdot e^{i(q\omega_0 (t+t_e))} \tag{2.30}$$

The constant c has been decomposed as $c = \omega_0 t_e$, where t_e, when considering equation 2.30, can be interpreted as the so called harmonic emission time [11].

t_e may in general be expressed as:

$$t_e^q = \frac{\partial \Phi_q}{\partial \omega} = \frac{1}{\omega_0} \frac{\partial \Phi_q}{\partial q} \tag{2.31}$$

In the case where Φ_q depends linearly on q, the emission time is constant for all harmonic orders, and no atto chirp will be present. If however $\Phi_q \propto q^2$, t_e will vary linearly with q, and each pulse in the pulse train will carry a small chirp b_{atto}, calculated as [9]:

$$b_{atto} = \frac{\partial^2 \Phi_q / \partial q^2}{\left(\partial \Phi_q / \partial q^2\right)^2 + 16 \left(\ln 2\right)^2 / \left(\Delta \omega\right)^4} \tag{2.32}$$

Chapter 3

Measurement of Short Pulses

As laser pulses shrink in length, the ability to measure them becomes increasingly important. There are a number of reasons for this. First, precise knowledge of the pulse properties is necessary for verifying theoretical models for pulse creation. Second, in order to make even shorter pulses, one must understand the distortions which limit the pulse duration. Third, when performing measurements using ultrashort pulses, their outcome might depend heavily on the pulse structure. In addition to this, it is always important knowing at least the pulse duration, in order to determine the time resolution of the experiment performed.

As already stated in the introduction of this thesis, measuring ultrashort light pulses introduces a not negligible amount of difficulties. These originate from the duration of the pulse as well as its frequency, if it is high enough. However, these are obstacles which more or less can be overcome. A number of techniques for ultrashort pulse characterization has been developed during the past decades, and this chapter will discuss some of these. Emphasis will be laid upon FROG [1], and its modifications XFROG [12] and FROG CRAB [13].

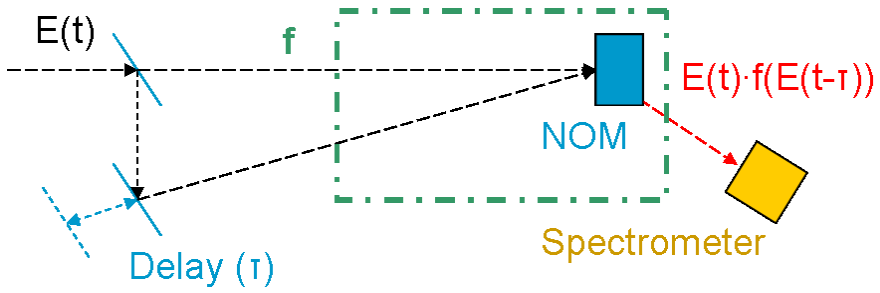

Figure 3.1: Basic outline of setup for FROG measurement.

3.1 Frequency-Resolved Optical Gating

The principle of FROG was first presented by Kane and Trebino in 1993 [1]. This is a technique which operate, not in the time or frequency domain, but in the 'time-frequency domain'. By introducing a nonlinear interaction between the pulse E one is interested in measuring, and a known or unknown 'gate' pulse G, one is able to 'slice' the pulse in time in order to study its spectral content as a function of time [14]. FROG can be regarded as a technique which spectrally resolves the signal pulse in any type of autocorrelation experiment performed in a nonlinear medium. From this time-frequency signal, one can in the end, by a so called FROG algorithm, yield the envelope and phase of the ultrashort pulses one intends to characterize.

3.1.1 Principle of FROG

The principle of an ordinary FROG setup is shown in figure 3.1. An incident light pulse $E(t)$ is split in two parts, which are made to propagate along different paths. Along the way, one of the beams is delayed in relation to the other. This delay, denoted as τ, is varied during the measurement process simply by moving the mirror which the beam is reflected by along the way of propagation. The structure of the two beams may also be manipulated in different ways along the way, if desirable. In for instance Polarization-Gate (PG) FROG, one of the pulses is sent through crossed polarizers, and the other through a half-wave plate in order to achieve a ± 45 deg linear polarization between the two pulses [14].

After the delay and manipulation stages, the two pulses are recombined in a nonlinear-optical medium (NOM) of some kind, for instance in a nonlinear crystal. The signal E_{sig} originating from the nonlinear process in the medium will be in the form of:

$$E_{sig}(t,\tau) = E(t) \cdot f[E(t-\tau)] = E(t) \cdot G(t-\tau) \tag{3.1}$$

f is a function which is defined by the manipulation stage as well as the nonlinear process in the medium of recombination. This function can be regarded as acting on the delayed pulse, and the resulting electric field is denoted as $G(t-\tau)$ which is called the gate. The gate is the parameter which distinguishes all the different variations of the FROG technique.

The final stage of the procedure is to measure the spectral intensity $S(\omega)$ of $E_{sig}(t,\tau)$ for each delay time step. This so called spectrogram is a two-variable dependent function, denoted $I_{FROG}(\omega,\tau)$, which is generally refered to as the FROG trace and written as [14]:

$$I_{FROG}(\omega,\tau) = \mathcal{F}[E_{sig}(t,\tau)] = \left| \int_{-\infty}^{+\infty} E(t) \cdot G(t-\tau) e^{-i\omega t} dt \right|^2 \tag{3.2}$$

The appearance of I_{FROG} will be different depending on which type of FROG (i.e. which type of gate) is being used. An example of a PG FROG trace, which

corresponds to $G(t-\tau) = |E(t-\tau)|^2$, can be seen in figure 3.2.

In a typical FROG measurement, the gate should preferably be shorter than the pulse one intends to measure. However, since the pulses one produces in the lab may be the shortest ones obtainable, this is not always possible. Furthermore, the gate shouldn't be infinitely short, since this would only yield the temporal intensity of the pulse. Correspondingly, if the gate would be a continuous wave, this would just yield the spectral intensity.

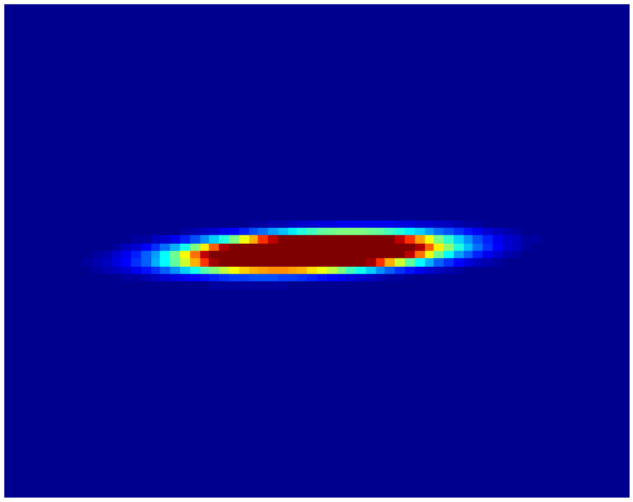

Figure 3.2: $I_{FROG}(\omega, \tau)$ for PG FROG. The y-axis corresponds to the angular frequency ω of $E_{sig}(t, \tau)$, and the x-axis to the delay τ.

3.1.2 Phase Retrieval

From I_{FROG}, one's desire is to retrieve both the envelope and phase function of the unknown pulse. In the beginning of FROG, using the pulse to gate itself in a spectrogram complicated the problem somewhat, since all the retrieval algorithms required knowledge of the gate function. The solution is to rewrite the expression in equation 3.2 as a two-dimensional Fourier transform [14]:

$$I_{FROG} = \left| \int_{-\infty}^{+\infty} E_{sig}(t,\tau) e^{-i\omega t} dt \right|^2 = \left| \int_{-\infty}^{+\infty} \hat{E}_{sig}(t,\Omega) e^{-i\omega t - i\Omega\tau} dt d\Omega \right|^2 \quad (3.3)$$

This expression can be verified by simple doing the integration with respect to Ω, which then yields equation 3.2. Here, one can see that the measured quantity is the squared magnitude of the 2D Fourier transform of $\hat{E}_{sig}(t, \Omega)$. Once $\hat{E}_{sig}$ is retrieved, one can simply obain $E(t)$, since $E(t) = \hat{E}_{sig}(t, \Omega = 0)$, if neglecting

a complex multiplicative constant k, which is of little interest:

$$\begin{aligned} \hat{E}_{sig}(t,\Omega) &= \frac{1}{2\pi}\int_{-\infty}^{+\infty} E_{sig}(t,\tau)\cdot e^{i\Omega\tau}d\tau = \frac{E(t)}{2\pi}\int_{-\infty}^{+\infty} G(t-\tau)\cdot e^{i\Omega\tau}d\tau \\ \hat{E}_{sig}(t,\Omega=0) &= \frac{E(t)}{2\pi}\int_{-\infty}^{+\infty} G(t-\tau)d\tau = k\cdot E(t) \end{aligned} \tag{3.4}$$

The integral on the second row is time independent, which one easy realise by performing a simple change of variables ($\tau' \rightarrow t-\tau$). Since the spectrogram measurement only yields the magnitude of the 2D Fourier transform of the desired quantity, the problem is then to find the phase of the Fourier transform of $\hat{E}_{sig}$. This is known as the 2D phase-retrieval problem.

Quite unintuitively, this is a solved problem when certain additional information regarding $\hat{E}_{sig}$ is available [14], such as it has finite support (that is, is zero outside a finite range of t and Ω). This is in contrast to the 1D equivalent, in which it is impossible to find one function of one variable whose Fourier transform-magnitude is known, despite additional information. Instead, the number of possible functions will be infinite. In ultrashort-pulse measurement, the required additional information consists of the knowledge of the mathematical form of the signal, given by the physics behind the manipulation stage and the nonlinear process used. For instance, in PG FROG, $E_{sig}(t,\tau) = E(t)|E(t-\tau)|^2$. This information turns out to, together with the Fourier magnitude, be sufficient for pulse reconstruction, and the problem is solved. Further, in chapter 4, a detailed description of the implementation of this solution into a working algorithm, will be discussed.

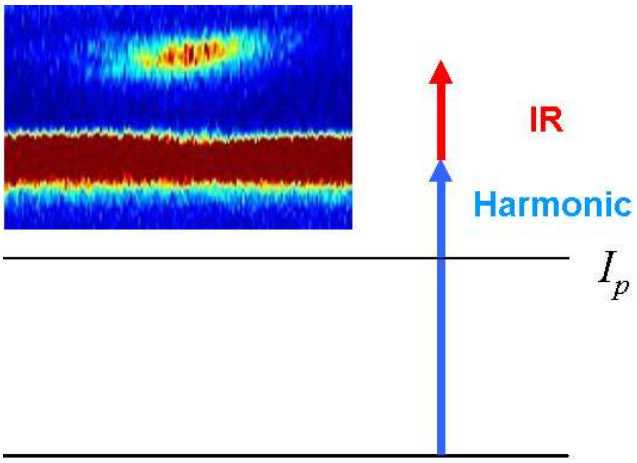

Figure 3.3: Photoelectron signal due to a high-order harmonic as well as stimulated absorption of an IR photon.

3.2 Cross-Correlation Frequency-Resolved Optical Gating

Although the time-frequency characterization of visible and infrared pulses by FROG is of no laborious task, it is nontrivial to extend it in to the XUV region. This is due to the difficulty of inducing nonlinear processes in this region. Techniques for acquiring FROG traces other than using a nonlinear optical medium must be used. The solution to this problem is to make use of the photoelectron signal due to cross correlation of harmonics and an infrared probe pulse in a gas medium. When the two pulses overlap in time, sidebands appear in the photoelectron spectrum [15], as seen in figure 3.3. This corresponds to the absorption of one harmonic photon together with aborption or emission of one or more IR photons.

The difference between XFROG and the 'ordinary' FROG method is the way the gate is constructed. In FROG $G(t) = f[E(t)]$, while XFROG demands no such relation between G and E. G is instead given by:

$$G(t) = \Lambda(t)(e^{i\omega_G t} + e^{-i\omega_G t}) \tag{3.5}$$

$\Lambda(t)$ simply denotes the envelope of the gate, while ω_G is the central frequency of the gate pulse. The $+\omega_G$ term represents the sideband due to absorption, and $-\omega_G$ is the emission term. ω_G is the central frequency of the gate pulse.

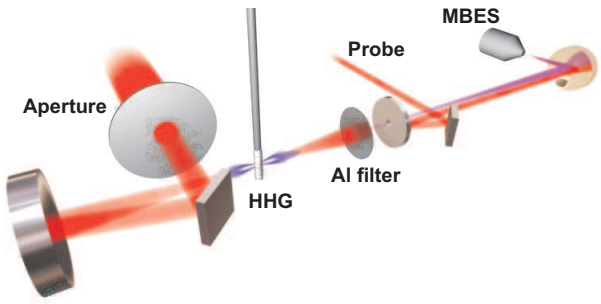

Figure 3.4: Setup for XFROG.

An example of an XFROG setup is shown in figure 3.4. The IR pulse in focused into a nozzle providing the noble gas used for HHG. When produced, the harmonics are made to propagate through an aluminium foil and a small aperture. This yields a spectrally as well as spatially filtered signal. The filtered harmonics and the IR probe are thereafter cross-correlated, ionising a gas (usually argon or neon), and the photoelectron spectrum is registered by a Magnetic Bottle Spectrometer (MBES).

An XFROG trace provides a good, intuitive picture of the pulse characteristics. From the length of the sideband, one can yield a resonably good understanding of the duration of the harmonic pulse. If the harmonic exhibits a chirp, this

will affect the sideband by tilting it somewhat. This is due to the fact that the energy variation due to the chirp of the harmonic, while the IR energy is unaffected, leads to a variation in energy of the sideband signal, as depicted in figure 3.5.

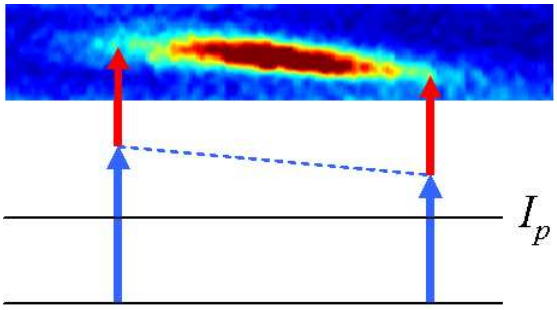

Figure 3.5: Negative chirp leading to a tilt in the sideband signal

3.3 Reconstruction of Attosecond Beating by Interference of Two-photon Transitions

While using the tilt of XFROG traces in order to deduce the harmonic chirp, the atto chirp between the harmonics can't be measured by this line of action. Instead, one can make use of sideband generation by cross-correlating the harmonics with the weak fundamental IR pulse. This method is called Reconstruction of Attosecond Beating by Interference of Two-photon Transitions (RABITT) [16], and is illustrated in figure 3.6. Since the distance between consecutive harmonics is $2\omega_0$, and the frequency of the IR pulse is ω_0, one sideband originating from stimulated absorption, and one from emission will overlap each other. This gives rise to interference effects, like the ones one acquires in Young's double slit experiment. Using second order pertubation theory, the sideband intensity I_S between harmonics q and $q+2$ is found to be proportional to a oscillating term as:

$$I_S \propto \cos(\Delta\Phi_{q+1} - 2\omega\tau) \tag{3.6}$$

$\Delta\Phi_{q+1}$ is used to denote the phase difference between the neighbouring harmonics: $\Phi_q - \Phi_{q+2}$. The RABITT experiment consists of studying the sideband signal as a function of the harmonic order q over a large range of harmonic orders. Thereby, one is able to determine the change of $\Delta\Phi_{q+1}$ with q, which in fact is a discretisized form of the second order spectral phase $\partial^2\Phi/\partial q^2$. From this and equation 2.32 the atto chirp can finally be calculated.

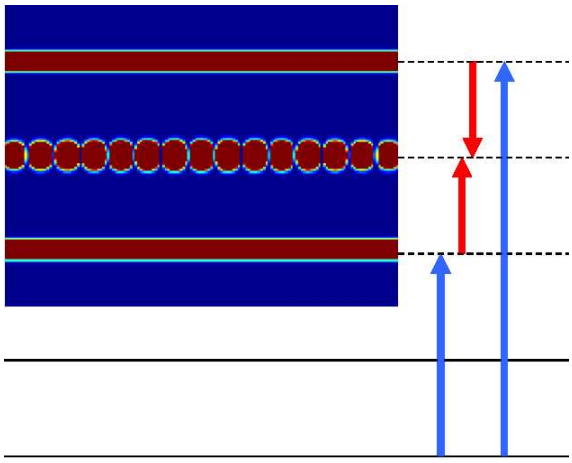

Figure 3.6: Two sidebands originating from two consecutive harmonics interfering with each other, giving rise to a RABITT signal.

3.4 Frequency Resolved Optical Gating for Complete Reconstruction of Attosecond Bursts

It is worth pointing out that while in many aspects similar, RABITT is not a FROG method. The point of RABITT is to introduce an interaction between consecutive harmonics, while FROG relies on the interaction between the harmonics and the gate pulse. It is however in principle possible to apply a FROG pulse retrieval algorithm to RABITT data, in order to fully characterize attosecond pulse trains. In this case, the scan must however be complete and cover the whole sidebands, otherwise the FROG algorithm will not have enough information for complete pulse reconstruction. Also, there is no longer any restriction on the strength of the IR pulse, since we no longer are speaking about any perturbative method, like RABITT is. This method is called Frequency Resolved Optical Gating for Complete Reconstruction of Attosecond Burst, or abbreviated: FROG CRAB [13], [17]. An example of a complete (simulated) FROG CRAB trace is shown in figure 3.7.

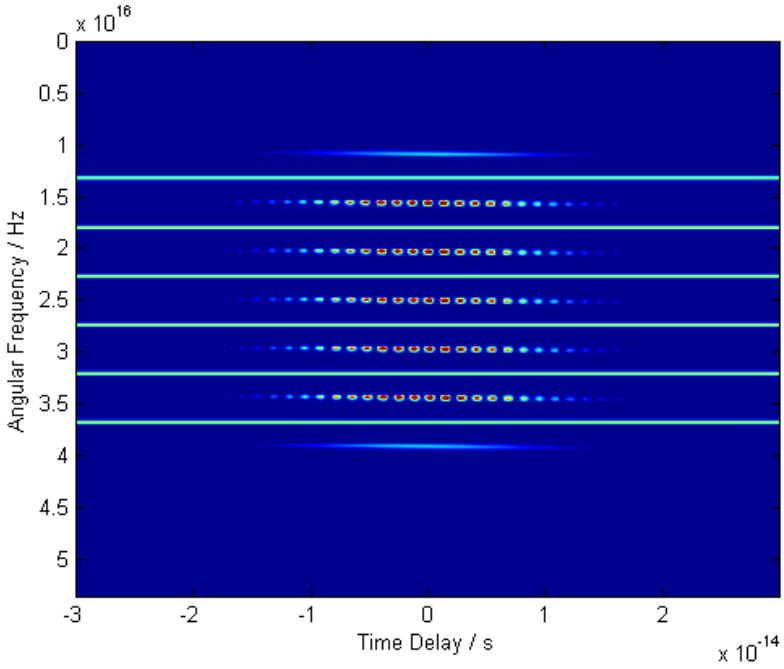

Figure 3.7: Simulated FROG CRAB trace, consisting of odd harmonics 17-27.

Chapter 4

The FROG Pulse Retrieval Algorithm

Even though rough information on the chirp and the duration of harmonics and attosecond pulses may be obtained by using methods like XFROG and RABITT, a more complete determination of the pulse envelope and phase behaviour is desirable. This chapter will describe the so called FROG pulse retrieval algorithms, from which FROG data is used to fully characterize ultrashort pulses by an iterative procedure. Emphasis will be laid on the Principal Component Generalized Projections Algorithm, PCGPA [18].

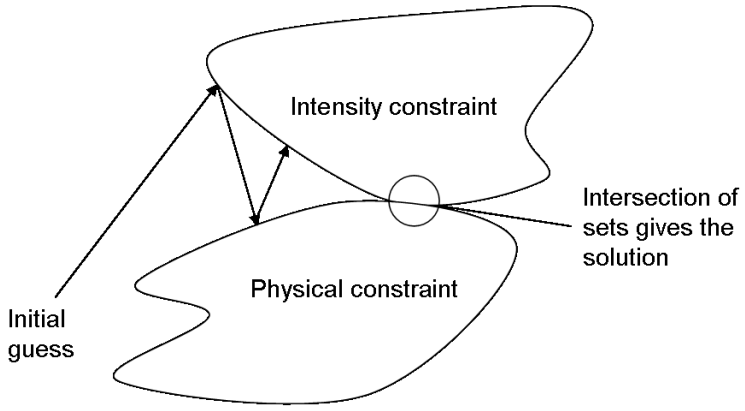

Figure 4.1: The ideal operation of a FROG inversion algorithm.

4.1 General FROG Algorithm Scheme

The purpose of the FROG algorithm is to calculate the pulse (or pulses) which gives rise to the FROG trace one has aquired in experiments, I_{FROG}. As seen

from equation 3.3, I_{FROG} is a real quantity from which no phase information can be extracted, and additional information is therefore needed. In the case of FROG, this comes from the form of $E_{sig}(t,\tau)$, which is expressed as $E(t) \cdot G(t-\tau)$.

The ideal operation of a FROG inversion algorithm is shown in figure 4.1. One starts with a suitable guess, which for instance may be random noise or a simple Gaussian. The final solution must satisfy two sets of constraints: 1) *The intensity constraint*, which corresponds to the set containing all functions which may build up I_{FROG} and, 2) *The physical constraint*, whose set contains all the functions which can be decomposed as $E \cdot G$. The aim is now to make the algorithm to alternate between the two constraints, converging to the solution, which – if there is one – is found at the point where the two sets intersect [14]. It should be noted that the picture in figure 4.1 merely is a rough sketch of the real interative process. First, the sets are not two-dimensional, and the algorithmic scheme takes instead place in a multidimensional functional space. Second, as can be seen in the picture, the sets are not necessarily convex. This means that unique convergence cannot be guaranteed. This may however in most pracical cases not be of any significant problem, since satisfying robustness of the algorithm can be achieved anyway.

The FROG error ϵ_{FROG} is defined as

$$\epsilon_{FROG} = \sqrt{\frac{1}{N^2}\sum_{i=1}^{N}\sum_{j=1}^{N}\left[I_{FROG}^{(k)}(\tau_i,\omega_j) - I_{FROG}(\tau_i,\omega_j)\right]^2} \tag{4.1}$$

where N is the size of the $N \times N$ matrix which builds up the FROG trace and (k) denotes the number of iterations made. ϵ_{FROG} thereby represents the rms error per element of the spectrogram. It is obviously essential to design the two constraint steps so that the FROG error is decreased for each iteration.

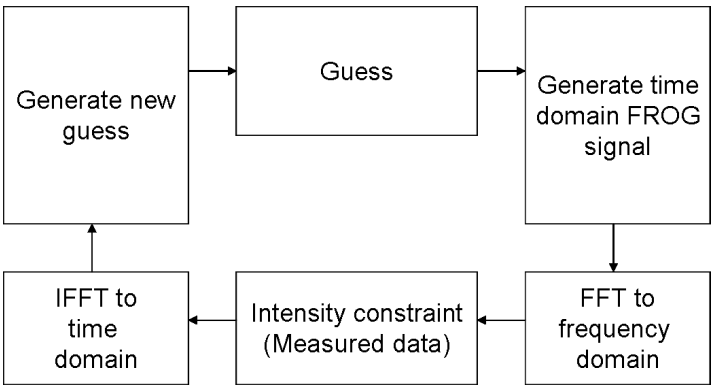

Figure 4.2: General scheme for a FROG inversion algorithm.

A general algorithmic scheme for alternation between the two set of constraints is shown in figure 4.2. One starts with an initial guess of the pulse (or pulses)

and from this guess generates a 2D FROG signal, first in the 'time-time domain' as $E_{sig}(t,\tau)$, and then by a 1D Fourier transformation in the time-frequency domain as $E_{sig}(\omega,\tau)$. After this, the intensity constraint is applied, which is done by simply replacing the magnitude of the FROG trace generated by the guess with the experimental FROG trace. Mathematically this is written as:

$$E_{sig}^{new}(\omega,\tau) = \sqrt{I_{FROG}(\omega,\tau)} \cdot \frac{E_{sig}(\omega,\tau)}{|E_{sig}(\omega,\tau)|} \tag{4.2}$$

The next step is to invert the new FROG trace back to the time-time domain. Afterwards a new guess is generated and sent back into the beginning of the next iteration cycle. This final step is meant to adjust the guess to the second, physical, constraint, and is basically what distinguishes all the different now existing FROG algorithms from each other.

Before moving on to the description of the PCGPA, a small discussion regarding the earlier FROG pulse retrieval algorithms will follow.

4.1.1 The Vanilla Algorithm

The original FROG inversion algorithm was the so called 'vanilla' or 'basic' algorithm [1]. It follows – like all the other FROG algorithms – the general outline in figure 4.2. Here the final step of each iteration is an integration of $E_{sig}(t,\tau)$ with respect to τ:

$$\int_{-\infty}^{+\infty} E_{sig}(t,\tau)d\tau = \int_{-\infty}^{+\infty} E(t)G(t-\tau)d\tau = E(t)\cdot\int_{-\infty}^{+\infty} G(t-\tau)d\tau \tag{4.3}$$

By a simple change of variables ($\tau' \to t-\tau$) one can see that the integration reduces to $C\cdot E(t)$, where C is a t-independent constant. Thus the next guess $E(t)$ is easily obtained from $E_{sig}(t,\tau)$. There are however significant problems using this method. While fast, the algorithm stagnates easily, resulting in high FROG error solutions. Also, the vanilla algorithm fails to invert complex functions like double pulses. In an attempt to overcome these problems, this algorithm was used to provide an initial guess to a brute force minimization of the rms error between the retrieved and the experimental FROG trace [19]. While this method is robust and in most cases do converge, it is however very slow.

4.1.2 The Generalized Projections Algorithm

With the method of generalized projections (GP), the FROG inversion algorithm made a big advance. The method originates from image analysis problems, but was in 1994 found to also be appliable to the FROG problem [20].

The solution is now found by making 'projections,' with geometrical analogues shown in figure 4.1. When projecting each guess onto the two sets, one ensures that the 'distance' between the guess and its projection is the shortest possible. A geometrical analogue would be to draw a line from the point outside the set

(representing the guess) to the border of the set so that the angle between line and border is right. The problem is now to find out which mathematical operations do correspond to projections with this property.

When dealing with the intensity constraint, it is found that simply replacing the magnitude of the FROG trace generated by the guess with the measured magnitude (as done in equation 4.2) is a generalized projection. When it comes to the second, physical, constraint, the procedure gets somewhat more tricky, though. The task is now shown to minimize the functional distance Z, defined by

$$Z = \sum_{i=1}^{N} \sum_{j=1}^{N} \left| E_{sig}^{(k)}(t_i, \tau_j) - E_{sig}^{(k+1)}(t_i, \tau_j) \right|^2 \tag{4.4}$$

where $E_{sig}^{(k)}$ is the FROG signal calculated in the earlier steps of iteration k, and $E_{sig}^{(k+1)}$ is the guess for the next cycle [20]. Taking into account the possibility of decomposing the signal as a product between pulse and gate gives $E_{sig}^{(k+1)}(t_i, \tau_j) = E^{(k+1)}(t_i) \cdot f\left[E^{(k+1)}(t_i - \tau_j)\right]$. In order to minimize Z one thus varies $E^{(k+1)}(t_i)$ until a minimum is found. In order to perform this minimization one therefore computes the direction of steepest descent: the negative of the gradient of Z with respect to the field $E^{(k)}(t_i)$. In practice, one must compute the derivative of Z with respect to each time-point in the complex field.

The advantages of the GPA with respect to the earlier algorithms are significant. First, it basically guarantees that the error always decreases for each iteration. Second, it is very robust. Third, it is much faster than the brute force minimization technique. And fourth, it converges very well in presence of noise [14]. There are however, as we shall see in the next section, algorithms of even better performance and properties.

4.2 The Principal Components Generalized Projections Algorithm

While the introduction of GPA proved to be a big step for the FROG inversion algorithm, an even larger step was made in 1997 with the introduction of the Principal Components Generalized Projections Algorithm (PCGPA) [18]. The main advantages compared to GPA are two: 1) The time-consuming and somewhat complicated minimization step is replaced by a simple multiplication of matrices, reducing the iteration time to a level which in some cases enables real time inversion of FROG traces, and 2) FROG traces consisting of pulse and gate functions independent of each other may be sucessfully inverted, where both pulse and gate is retrieved. Such an algorithm is refered to as a blind-FROG inversion algorithm, since it makes no a priori assumptions about the relationships between the pulse and the gate.

4.2.1 The Outer Product Form Matrix

The main element of PCGPA is the so called Outer Product Form Matrix (hereafter abbreviated as the OP matrix). This matrix is easily constructed by two vectors – one representing the unknown pulse and the other one the gate – and the PCGPA is based on certain properties specific for this OP matrix.

In order to make an OP matrix one first has to define the pulse and the gate vector. Suppose $E(t)$ and $G(t)$ being sampled at given values of t with a constant spacing of Δt. Then $E(t)$ and $G(t)$ can be thought of as vectors of length N whose elements sample E and G at discrete times:

$$E = \left[E\left(-\frac{N}{2}\Delta t\right), \ldots, E\left(\left(\frac{N}{2}-1\right)\Delta t\right)\right] = [E_1, \ldots, E_N] \tag{4.5}$$

$$G = \left[G\left(-\frac{N}{2}\Delta t\right), \ldots, G\left(\left(\frac{N}{2}-1\right)\Delta t\right)\right] = [G_1, \ldots, G_N] \tag{4.6}$$

The OP matrix O is now defined as [18]:

$$O = \begin{pmatrix} E_1G_1 & E_1G_2 & \ldots & E_1G_N \\ E_2G_1 & E_2G_2 & \ldots & E_2G_N \\ \vdots & \vdots & \ddots & \vdots \\ E_NG_1 & E_NG_2 & \ldots & E_NG_N \end{pmatrix} \tag{4.7}$$

This matrix contains all the points required to construct the time domain FROG trace because it contains all the interactions between the pulse and the gate for each discrete time delays. (For instance, the main diagonal of O above can easily be identified as being the FROG signal at $\tau = 0$.) The OP can therefore be transformed into the FROG trace, and the trace can in the same manner be transformed back to the OP matrix again.

The rows and columns of the OP matrix may be manipulated to generate an equivalent matrix that gives a time domain representation of the FROG trace. By leaving the first row unshifted, shifting the second row one step to the left, the third two steps and so on, one obtains the following matrix:

$$\begin{pmatrix} E_1G_1 & E_1G_2 & E_1G_3 & \ldots & E_1G_{N-2} & E_1G_{N-1} & E_1G_N \\ E_2G_2 & E_2G_3 & E_2G_4 & \ldots & E_2G_{N-1} & E_2G_N & E_2G_1 \\ E_3G_3 & E_3G_4 & E_3G_5 & \ldots & E_3G_N & E_3G_1 & E_3G_2 \\ E_4G_4 & E_4G_5 & E_4G_6 & \ldots & E_4G_1 & E_4G_2 & E_4G_3 \\ \vdots & \vdots & \vdots & \ddots & \vdots & \vdots & \vdots \\ E_NG_N & E_NG_1 & E_NG_2 & \ldots & E_NG_{N-3} & E_NG_{N-2} & E_NG_{N-1} \\ \tau = 0 & \tau = -1 & \tau = -2 & \ldots & \tau = +3 & \tau = +2 & \tau = +1 \end{pmatrix} \tag{4.8}$$

Now one sees that all columns of this new matrix contains the FROG signal $E_{sig}(t, \tau)$ for all different delay times, as indicated below the matrix. By simply rearranging the columns so that the most negative τ is to the left and the most positive is to the right, a discretized FROG signal in the time-time domain

may be made. In order to get the signal in the time-frequency domain one simply Fourier transforms each column. By finally taking the magnitude of this complex result, the FROG trace one measures in experiments is produced. The whole procedure is illustrated in figure 4.3.

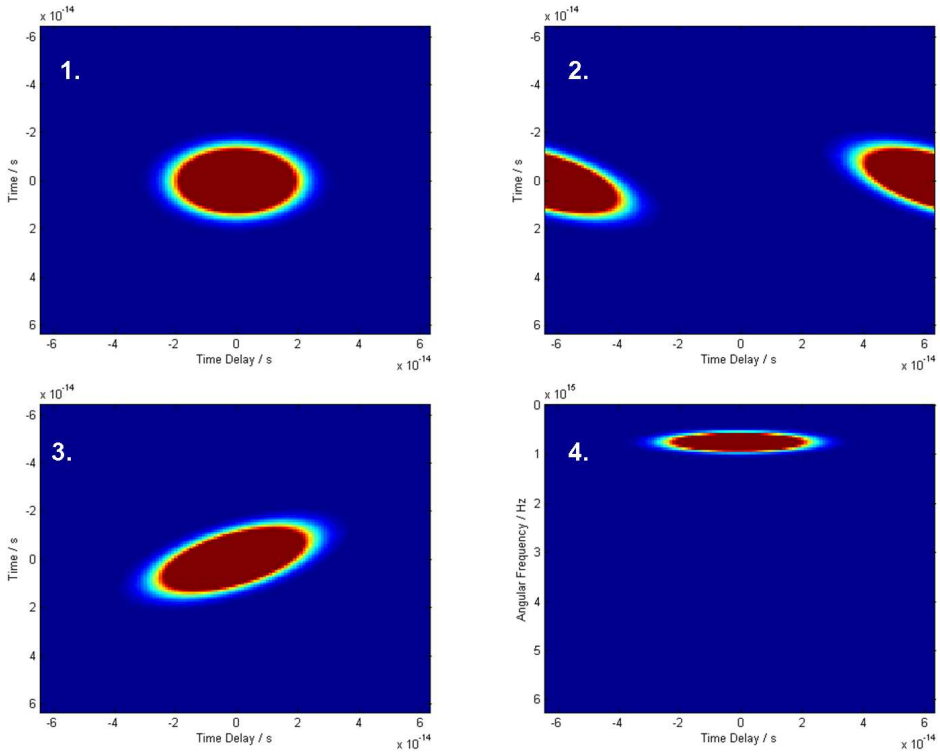

Figure 4.3: The different steps in manipulating the OP matrix into a time-frequency FROG trace. Figure 1) plots the modulus of the OP matrix. In 2) the OP matrix after row manipulation is drawn. This corresponds to the matrix in equation 4.8. 3) represents the matrix after being manipulated columnwise and is therefore now the FROG signal in the time-time domain. And finally, in 4), each column is Fourier transformed, giving rise to the FROG trace in the time-frequency domain.

4.2.2 PCGPA inversion

We have now shown that the OP matrix may be used to form a matrix containing a discrete version of the FROG trace (and vice versa). We will noe use properties specific to the OP matrix in order to retrieve both E and G.

While it is easy to imagine an infinite number of complex images that have the same magnitude as the FROG trace we wish to invert, there is however only one image with the same magnitude which can be formed by the outer product of a *single pair of nontrivial vectors* [18]. In order to find the proper vector

pair (that is, the pulse and the gate) the phase of the spectrogram must be determined using a 2D phase retrieval algorithm. When we have the phase, we can simply decompse the OP matrix in the pair of vectors which is originally was composed of.

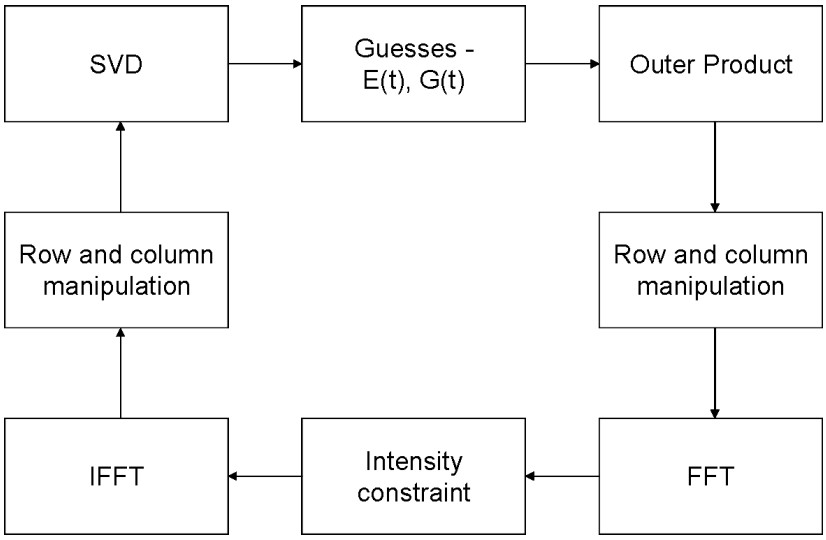

Figure 4.4: The general PCGPA scheme. Each step is more thourougholy explained in the text.

The PCGPA works in the same way as all the other inversion algorithms, as depicted in figure 4.2. As in all the earlier algorithms, the step that differs from the others is the last one, where the new guess is being generated. However, a more detailed insight in how the PCGPA works is shown in figure 4.4. The procedure is as follows:

1. The initial guesses of pulse and gate are made, and an OP matrix is formed by these two guesses.
2. By row and column manipulation, $E_{sig}(t, \tau)$ is formed.
3. By Fourier transformation one obtains $E_{sig}(\tau, \omega)$.
4. The magnitude of $E_{sig}(\tau, \omega)$ is replaced by the magnitude of the FROG trace.
5. By the inverse Fourier transform followed by row and column manipulation the matrix is converted back into its OP form again. A final *singular value decomposition* step (SVD) is applied in order to generate the new guess.

The final step has to be explained more thourougholy. When converted back into its OP form, the matrix no longer exhibits the features of a real OP, since its magnitude has been replaced with another. One now has to find the best real-OP approximation of the matrix, in order to send it back into the beginning of the iteration.

One important property of a real OP matrix is that it has one and only one nonzero eigenvalue; that is, its rank is equal to one. The eigenvector of such a matrix is E, the pulse. Correspondingly, the complex conjugate of the eigenvector of the transpose of the OP matrix is the gate, G. If the matrix after being molded by the intensity constraint is the correct FROG trace it is thus a simple task to obtain both the pulse and the gate out from this matrix. If not, one must find the best rank-one approximation of the new matrix, which is just a different way of saying what was written in the previous paragraph. The answer to this problem is not a direct minimization step, but a certain kind of decomposition – the SVD. SVD decomposes an arbitrary $N \times N$ matrix A into three new matrices U, W and V:

$$A = U \cdot W \cdot V^T \tag{4.9}$$

Both U and V are orthogonal square matrices and W is a square diagonal matrix, with diagonal elements $w_1, w_2, \ldots, w_N$. The matrix A can thus be regarded as being decomposed into a superposition of OP matrices $O_1, O_2, \ldots, O_N$, weighed by the elements of W:

$$A = w_1 \cdot O_1 + w_2 \cdot O_2 + \ldots + w_N \cdot O_N \tag{4.10}$$

All of the possible O_i correspond to OP matrices formed by possible pulse vectors (columns of U) and gate vectors (rows of V^T). The best OP approximation of A would thus be the OP matrix which corresponds to the largest weighting factor w_l, and is composed of the elements in the corresponding column of U and row of V^T. In fact, keeping this *principal component* for the next iteration of the algorithm, is found to be a minimization of the error function

$$\epsilon^2 = \sum_{i=1}^{N} \sum_{j=1}^{N} \left| A^{i,j} - E^i G^j \right|^2 \tag{4.11}$$

which can be seen as an analogue to the minimization step of the GP algorithm.

While the SVD method is quite intuitive, it contains lots of unnecessary calculations, since there basically is only one vector pair corresponding to the largest weighting factor which is needed. This makes the calulations somewhat time consuming. Fortunately, the principal vector pair which builds up the dominant OP matrix may be found directly with much less computation, reducing the SVD step to simple matrix-vector multiplications [21], [22].

The SVD routine calculates the eigenvectors E_i of AA^T, which are the columns of U, and the eigenvectors G_i of A^TA, which are the columns of V:

$$AA^T E_i = \lambda_i E_i \tag{4.12}$$

$$A^T A G_i = \lambda_i G_i \tag{4.13}$$

The sets E_i and G_i are both orthonormal, and the eigenvalues λ_i are found to be related to the weighting factors by $\lambda_i = w_i^2$. Equation 4.10 can be expressed as:

$$A = \sum_{i=1}^{N} \sqrt{\lambda_i} E_i G_i^T \tag{4.14}$$

λ_i, E_i and G_i are all provided by the SVD, but one only needs the vector pair corresponding to the largest $|\lambda_i|$. Suppose there is an arbitrary nonzero $1 \times N$ vector x. Since the eigenvectors of AA^T form an orthonormal set, this vector may be expressed as a superposition of E_i.

$$x = \sum_{i=1}^{N} \kappa_i E_i \tag{4.15}$$

where κ_i is a set of constants. If one multiplies x with AA^T and takes equation 4.12 into account one gets:

$$AA^T x = \sum_{i=1}^{N} AA^T \kappa_i E_i = \sum_{i=1}^{N} \kappa_i \lambda_i E_i \tag{4.16}$$

AA^T can be thought of as an operator that maps x onto a superposition of eigenvectors. Because $AA^T \kappa_i \lambda_i E_i = \kappa_i \lambda_i^2 E_i$ multiplying equation 4.16 by $(AA^T)^{p-1}$ gives

$$\left(AA^T\right)^p x = \sum_{i=1}^{N} \kappa_i \lambda_i^p E_i \tag{4.17}$$

As p becomes large, the largest eigenvalue λ_l (that is, the largest weighing factor w_l) dominates the sum so that $\left(AA^T\right)^p x \approx \kappa_l \lambda_l^p E_l$. This method is called *the power method*. By simply normalizing the result one gets when multiplying repetively, E_l is obtained. Since this is the eigenvector corresponding to the largest eigenvalue, this approximately equals the next guess for the pulse, $E^{(k+1)}$. Since x is assumed to be an arbitrary vector one may as well multiply the previous guess $E^{(k)}$ with AA^T in order to calculate $E^{(k+1)}$. While better approximations for the eigenvector can be made by using this operation several times per iteration, once per iteration ($p = 1$) is adequate in practice. Correspondingly, since G_i are the eigenvectors of $A^T A$, the next guess for the gate is made by multiplying the previous guess of the gate by $A^T A$.

Chapter 5

Implementation of the PCGPA

The main aim of this diploma project has been to write a FROG pulse retrieval algorithm based on the theories which have been presented in previous chapters. The algorithm which I have written is based on the PCGPA and is presented in appendix A.

Before applying the algorithm on measured data, it is of extreme necessity to first test its performance on simulated, already characterized, data. Would the results of this test be too disappointing, one obviously cannot rely on any results obtained using experiments. We will first examine how well the PCGPA behaves when retrieving pulses from simulated XFROG traces, and thereafter, the algorithm will be tested on experimental XFROG data. In the end of this chapter, we will attempt to characterize both simulated and real attosecond pulse trains.

5.1 XFROG Implementation

In the following sections, important characteristics of the PCGPA will first be examined using simulated XFROG traces. Since we already know what the outcome of these test runs should be, possible flaws of the algorithm can be detected and perhaps even solved, by adding improvements to the original program. By changing certain parameters, such as the rate of the data lowpass filtering, we also can get some understanding of if and how the pulses retrieved are affected by these. All this knowledge will be of great importance when we, in the end of this section, apply the PCGPA to experimental XFROG data.

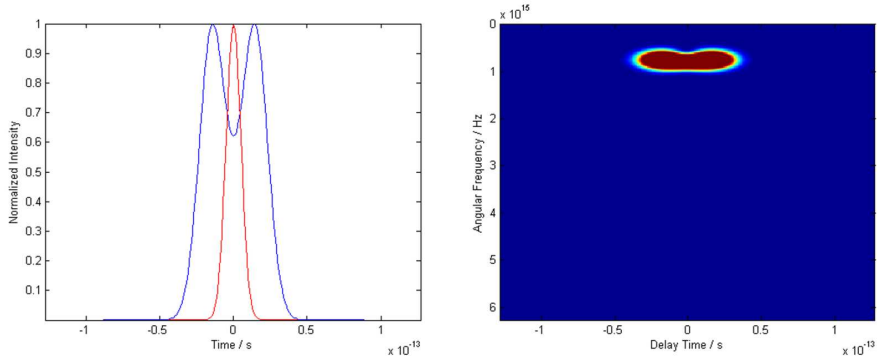

Figure 5.1: To the left: Femtosecond double pulse (blue) and the gate pulse. To the right: Their simulated XFROG trace.

5.1.1 Implementation on Simulated Data

Two tests of the PCGPA on simulated data will now be performed: In the first we will try to retrieve an unchirped double pulse, and in the second test a more complex pulse, exhibiting a significant amount of chirp.

The Double Pulse Test

To illustrate the main properties of the algorithm, we start with a simple double pulse which is shown in figure 5.1. Its central wavelength is 40 nm and its FWHM is about 50 fs; it is also unchirped. Shown in the same figure is the gate pulse, which exhibits a wavelength of 800 nm, an FWHM of 12 fs and no chirp. The corresponding XFROG trace is made by using the OP matrix procedure as described in the previous chapter.

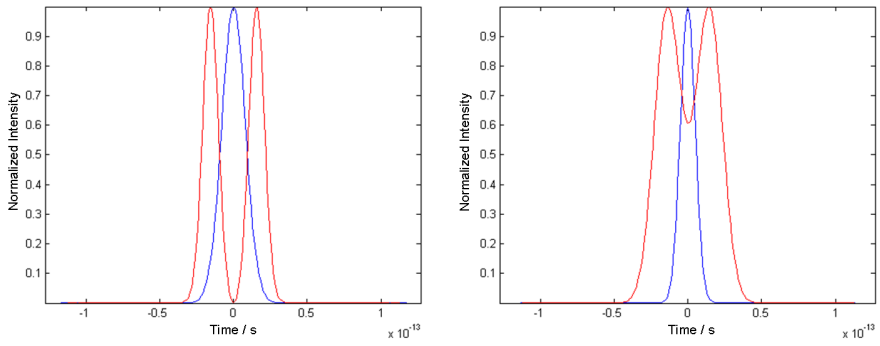

Figure 5.2: To the left: Retrieved pulse (blue) and gate (red) without spectral constraint. To the right: Retrieved pulse (blue) and gate (red) with spectral constraint.

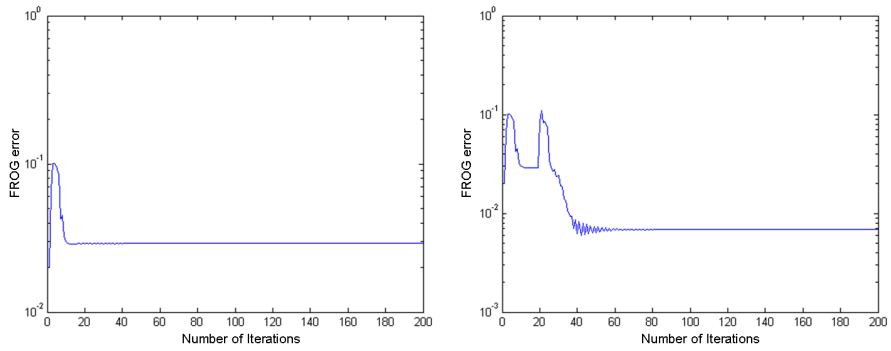

Figure 5.3: To the left: FROG error as a function of iteration number for the pulse in 5.1 without spectral constraint. To the right: FROG error as a function of iteration number for the pulse in 5.1 with spectral constraint.

What happens if we run the simulated XFROG trace in our inversion algorithm? The result is shown to the left in figure 5.2, and is not satisfying at all; the retrieved pulse looks more like the real gate, and vice versa. However, even with this in mind, the algorithm doesn't seem to act properly: The double pulse is a little bit too thin and the single pulse is too broad. In figure 5.3, to the left, one can see that the FROG error (defined by equation 4.1) stagnates somewhere in the middle of 10^{-1} and 10^{-2}. This is too high to be acceptable.

In order to make the results of the algorithm more accurate, it is possible to apply some sort of additional constraints to the iteration process. One such constraint may be the spectrum of the pulse one wants to characterize. After all, all one needs to measure the spectrum is a simple spectrometer and one doesn't need to worry about the diffuculties with time resolution at all. Also, the implementation of this constraint is simple: At some point in the algorithm one just replaces the spectrum of the guess with the spectrum of the real pulse. It should be noted that this additional constraint is not a part of the theory of projections which was gone through in the previous chapter; it is simply a 'practical' add-on constraint which empirically has been found to be useful.

During this project it has been found that one must be very careful with where and how often one performs this replacement. Using this procedure once every iteration causes the algorithm to go berzerk, leaving just nonsense data as result. The optimum procedure is to replace the spectrum *only once* somewhere in the beginning of the algorithm, for instance in the 20th iteration step. Applying this to the double pulse test, the pulses retrieved look like what is shown to the right in figure 5.2. Still, there is a mix-up (whose specific origin is somewhat mysterious), but apart from that the pulses retrieved look pretty much like the pulses we started from. To the left in figure 5.3 we also see that imposing the additional spectral constraint at iteration number 20, forces the FROG error to go down below 10^{-2}. From now on, the PCGPA will always use a spectral constraint, when a spectrum is available.

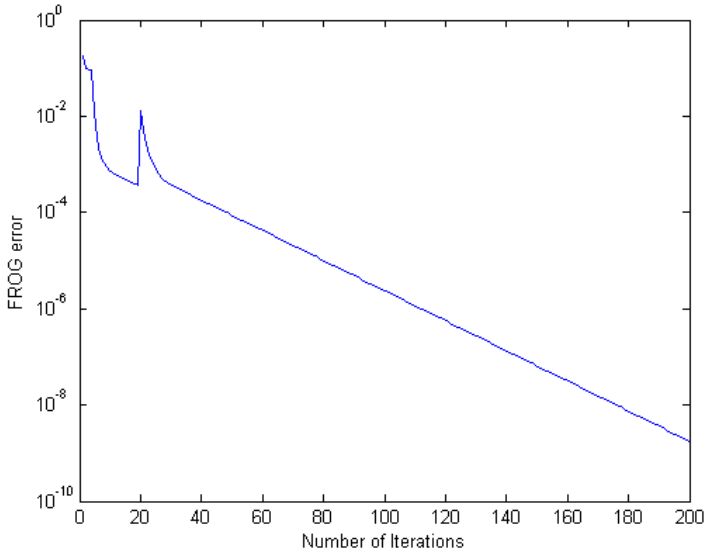

Figure 5.4: Plot over the FROG error as a function of iteration number when retrieving a double pulse using a forced gate.

If one regards the gate pulse already being satisfyingly characterized, there is no need for a blind-XFROG algorithm. Then one doesn't have to bother about guessing the gate anymore, and may just force the gate by inserting the real one for each iteration. Doing so in the double pulse case, eliminates the mix-up problem, and also reduces the FROG error by several factors of ten, as seen in figure 5.4.

The Chirped Harmonic Sideband Test

Let us now test the algorithm using more complex, asymmetrical pulses. In figure 5.5 a simulated sideband originating from a highly chirped 19th harmonic is represented, together with the gate pulse used in the previous example. The numerical simulation of the sideband has been designed to mimic the experimental conditions in an XFROG experiment as closely as possible. When inserting the XFROG trace to the right in the figure into our algorithm, we get a result which is presented in figure 5.6. This is, maybe somewhat unexpected, an almost perfect match with the pulses we started with. This is confirmed by looking at the FROG error, which is shown in figure 5.7, where we can see that it after not even 200 iterations stagnates on an error of the magnitude of 10^{-6}! Also, what is shown to the right in figure 5.6 is a comparison of how the instantaneous frequency (that is, $d\Gamma(t)/dt = \omega(t) = \omega_0 + d\Phi(t)/dt$) varies with respect to both the 'real' and the retrieved harmonic. The shapes of the graphs are more interesting than the actual values they represent since we are not interested in deciding the value of ω_0, but rather in getting a picture of the behaviour of $d\Phi(t)/dt$. (The reason why ω_0 is different in the two plots is because the time

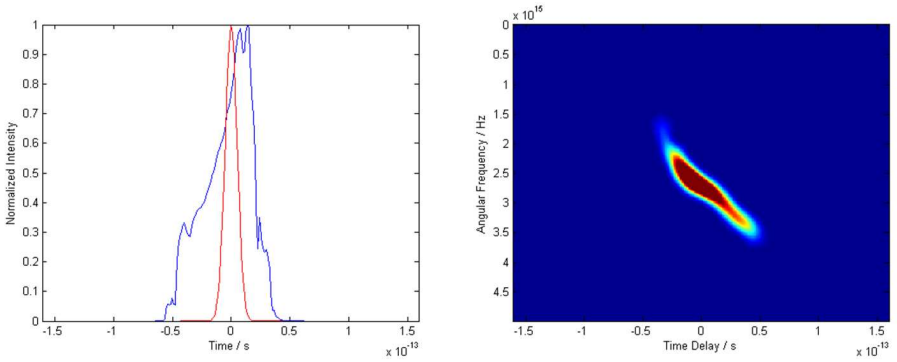

Figure 5.5: To the left: Simulated 19th harmonic with a high negative fundamental chirp (blue) an an unchirped gate pulse (red). To the Right: Their simulated XFROG trace.

resolution we use in our simulations is not high enough to fully resolve the correct frequency.) Thus, the agreement between the two plots is excellent.

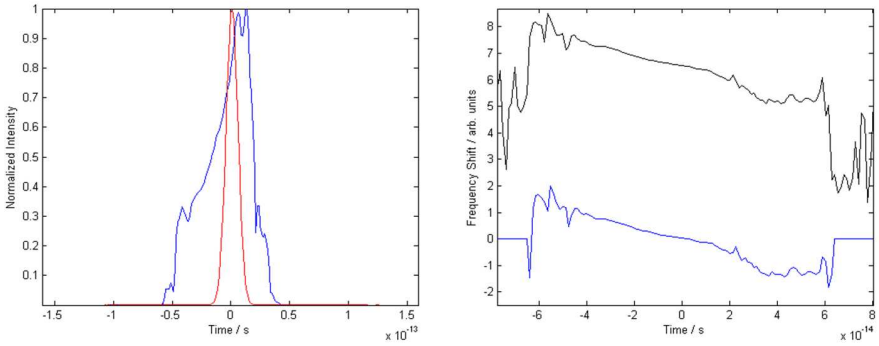

Figure 5.6: To the left: Retrieved harmonic (blue) and gate (red). To the right: Frequency variation of the real harmonic (blue) and of the retrieved (black).

One could now ask oneself why we get better results when trying to retrieve more complex pulses. The answer probably lies in the lack of symmetry of the pulses retrieved, as well as in possible similarities between the pulse and the gate. When dealing with symmetric pulses which also have a structure with high resemblence to the gate, dangerous pitfalls suddenly appear: The chance of mixing up pulse and gate is highly increased, and weird 'mean value pulses' give rise to FROG traces which almost cannot be distinguished from the real FROG trace at all. Asymmetric pulses with little resemblence to the gate however seem to eliminate many of these 'false' solutions.

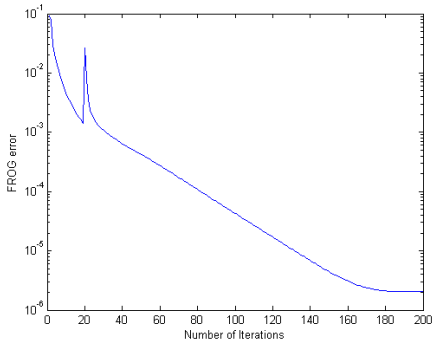

Figure 5.7: FROG error for the harmonic presented in figure 5.5.

5.1.2 Implementation on Experimental Data

We now turn to the 'real' world, to examine if the PCGPA also is able to retrieve pulses from experimental XFROG traces. Measurements of harmonics by the XFROG method have earlier been performed at the Lund Institute of Technology, by Mauritsson *et al.* in 2004 [23], using the setup shown in figure 3.4. Harmonics were generated by 815 nm IR pulses with durations between 35 and 90 fs. Scans were done under five different experimental conditions, labeled (a)-(e): Harmonic generation with a negative chirp on the fundamental – case (a) and (b) – generation with no fundamental chirp – case (c) – and finally a positive fundamental chirp in (d) and (e). Since the fundamental is transfered to the harmonics as described by equation 2.28, the harmonics will exhibit each different chirp rate b.

An example of what such an experimental XFROG scan looks like is given in figure 5.8. It is of importance to realise that each visible sideband is a mixture of two sidebands, since the distance between consecutive harmonics is $2\omega_0$ and the frequency of the gate pulse is ω_0. This means that the sideband originating from absorption of an IR photon in harmonic $n-1$, will be mixed with the sideband due to emission in harmonic $n+1$. Thus, processing a sideband n in an XFROG scan like the one shown in figure 5.8 will only give the mean duration and chirp of harmonics $n-1$ and $n+1$. For example, the sideband labeled 18 originates both from harmonic 17 and 19. The sidebands shown in the figure are sidebands 14-22 (with sideband 24 very faintly hinted far to the right).

By simply measuring the sideband length and tilt, Mauritsson *et al.* have calculated both the duration of the harmonics, as well as their chirp. In table 5.1 the determined duration and chirp are indicated for sideband 18 in the five cases. The harmonic duration $\Delta\tau$ is obtained from the duration of the sideband $\Delta\tau_{sb}$ according to $\Delta\tau = \sqrt{(\Delta\tau_{sb})^2 - (\Delta\tau_{IR})^2 - (\Delta\tau_{geo})^2}$, where $\Delta\tau_{IR}$ is the infrared gate pulse duration, and $\Delta\tau_{geo}$ is a geometrical factor which is meant to compensate the fact that the two beams, as can be seen in figure 3.4, are not collinear, but intersect each other by a small angle. This factor is estimated

	$\Delta\tau/fs$	$b/10^{27} \cdot s^{-2}$
(a)	41	-14
(b)	31	-11
(c)	23	-10
(d)	28	10
(e)	36	13

Table 5.1: Values of harmonic duration and chirp for five different cases (a)-(e) of harmonic 18, measured by Mauritsson *et al.*.

to be about 18 fs. Further, the chirp rate can be calculated from the sideband chirp b_{sb} by $b = b_{sb}\left[1 + \left((\Delta\tau_{IR})^2 + (\Delta\tau_{geo})^2\right)/(\Delta\tau)^2\right]$.

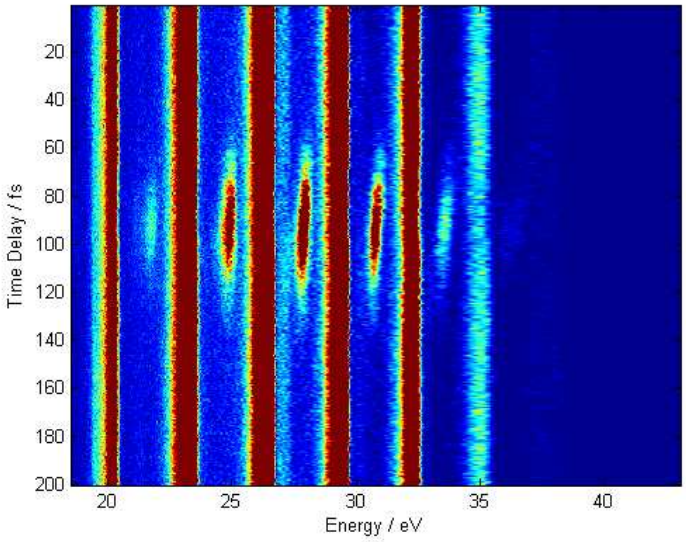

Figure 5.8: Example of an XFROG scan.

We applied the PCGPA to the experimental data. The intention was, by using the blind-FROG algorithm presented in appendix A, to determine both the pulse and the gate from the same measurement. This proved however to be a nearly impossible task, since severe problems soon came up. Since the gate pulse already had been fairly characterized by other techniques as a Fourier limited 12 fs long pulse, the outcome of the test could partially be predicted. In a few cases, running the blind-FROG algorithm gave the expected gate as a result, but in an equal number of test runs, it did not. Like in the previous double pulse-test, pulse and gate seemed to be mixed with each other – in some cases they even looked identical (when expected not to be). In addition to that, the algorithm never seemed to converge properly, at best stagnating on FROG errors in the region of about 5%.

Some of these ambiguities might have been eliminated if a spectral constraint had been added. However, when performing the cross-correlation experiment, the spectrum of the harmonics was never measured, making this solution unavailable. However, one possibility remained: By regarding the gate as fully characterized as a Gaussian Fourier limited pulse with an FWHM of 12 fs and a wavelength of 815 nm, it would be possible to 'force' the gate in each iteration, thereby – if the gate had been characterized correctly – making the algorithm to properly converge. This actually proved to be a seemingly better solution, since the PCGPA now in every case converged at FROG errors between 0.6 and 2%.

Figure 5.9 shows the retrieved envelope and phase information calculated from sideband 18(b). In the figure, the phase information is given by plotting $d\Gamma/dt = \omega_0 + bt$. In order to determine the value of b, one fits a polynomial of the first degree to the data points in the neighbourhood of the pulse. The value of the slope of this polynomial then directly gives b. Figure 5.10 shows sideband 18 for cases (a)-(e), together with the calculated values of b. This indicates that at least the results of the algorithm are qualitatively good, since a sideband tilting in one direction gives rise to a b with opposite sign as the sideband which tilts in the other direction.

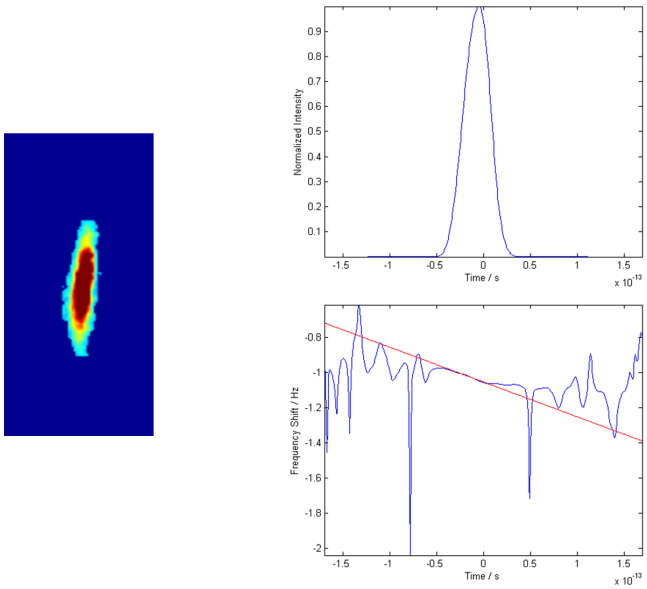

Figure 5.9: Left: Sideband 18(b). Center: Retrieved pulse with an FWHM of 33 fs. Right: Retrieved frequency shift (blue), with a first-degree polynomial fitted to the values of relevance (red). $b = -3.17 \cdot 10^{27} s^{-2}$ and $\epsilon_{FROG} = 0.0077$.

Even though we get good qualitative results when calculating b by PCGPA, this is of course not enough. In order to get some idea of the quality of the algorithm as a quantitatively good method we must compare our values with trustworthy

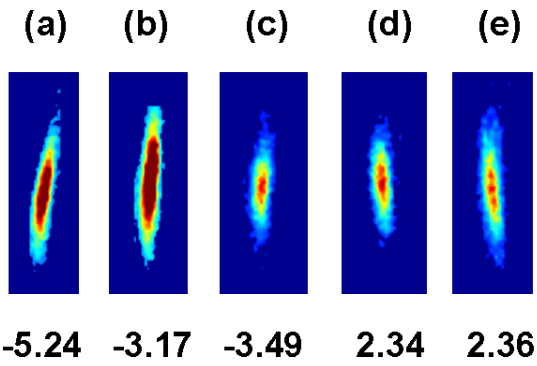

Figure 5.10: Sideband 18 (a)-(e). Below are the PCGPA calculated harmonic chirp rates b for each sideband written, given in $10^{27}s^{-2}$.

	$\Delta\tau/fs$	$b/10^{27} \cdot s^{-2}$	ϵ_{FROG}
(a)	42	-5.24	0.0090
(b)	33	-3.17	0.0077
(c)	28	-3.49	0.0082
(d)	31	2.34	0.0083
(e)	41	2.36	0.0100

Table 5.2: Values of harmonic duration and chirp rate for harmonic 18(a)-(e), calculated by the use of the PCGPA. Also, in the third column, the FROG error for each calculation is shown.

results obtained by using a different method. Once again, we look at Mauritsson *et al.* [23]. Table 5.2 shows PCGPA-calculated FWHM:s and chirp rates for sideband 18(a)-(e). These can be compared with what was previously found in table 5.1. While the duration of the pulses seem to agree fairly well with the previous results, the values of b however do not. The ratios between the chirp rates seem to be pretty much the same when comparing the first measurement to the other; however, their absolute values do not agree at all.

This fact becomes even more clear when making a second comparison, where b for cases (a)-(e) is plotted as a function of the harmonic order q. Figure 5.11 is a plot over the PCGPA calculations, and figure 5.12 is a plot over the values found in Mauritsson *et al.* Both plots do have a striking resemblance in shape, but, however, not in absolute values. The reason for this remains a mystery, though it should be noted that the values measured by Mauritsson *et al.* probably are the most correct ones, since they are very similar to what has been calculated in simulations.

A number of possible errors may be due to the model of the electric field that the algorithm is based on, which totally neglects the spatial dependence of the field. First, the noncollinearity of the beam geometry might give rise to errors. When running the algorithm, this is taken into account for by in the inversion replacing

the duration of the gate pulse $\Delta\tau_{IR}$ with a duration of $\sqrt{(\Delta\tau_{IR})^2 + (\Delta\tau_{geo})^2}$, which approximately is equal to 22 fs. This might however not be enough to fully compensate the lack of collinearity in the geometry, and a expanded version of the PCGPA which treats this problem more rigorously might be needed. In order to get an idea of how big the error might become if neglecting the beam geometry, the calculations which was done in Mauritsson *et al.* was made once again, but this time with the geometrical factor set to zero. This reduced the chirp rates with in general 20%, which is not enough to fully explain the results obtained in this thesis, but may be worth having in mind.

Also, when only looking at the temporal aspects of the pulse and the gate, one considers the two fields as being in the form of plane waves. This is however not entirely true, and a model based on spherical fields might give better results. There has however during this project unfortunately not been time to develop this idea into more than just an idea.

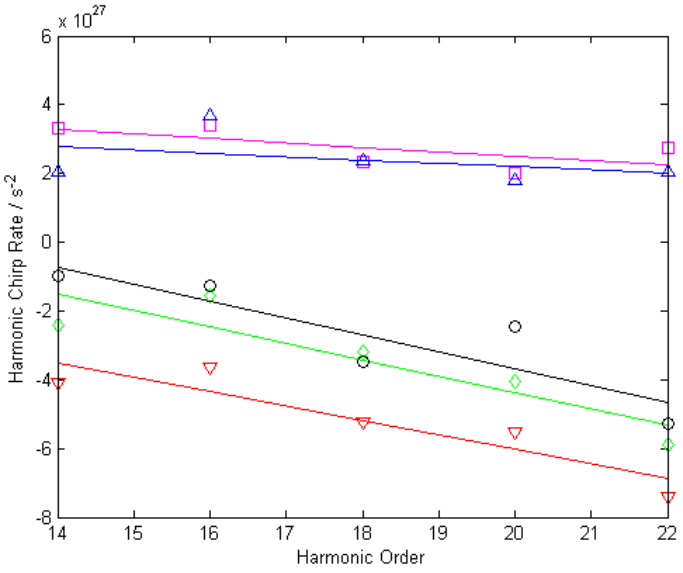

Figure 5.11: Harmonic chirp rate calculated by PCGPA plotted as a function of harmonic order. Red colour – case (a); green – (b); black – (c); (d) – purple; (e) – blue.

The treatment of the FROG trace before sending it into the algorithm is another possible source of errors. While the algorithm in principle is relatively stable against noise, the data must yet undergo some threshold and lowpass filtering. The biggest problem in this aspect is the influence of the adjacent harmonics, which in some cases is so large that parts of the sideband are overshadowed and take on a distorted appearance in the eyes of the algorithm. In order to make the PCGPA to converge at all, one must filter out a certain amount of this distorting background. By doing so it is however very likely that parts of the information on the sideband itself are lost. Simulations which have been

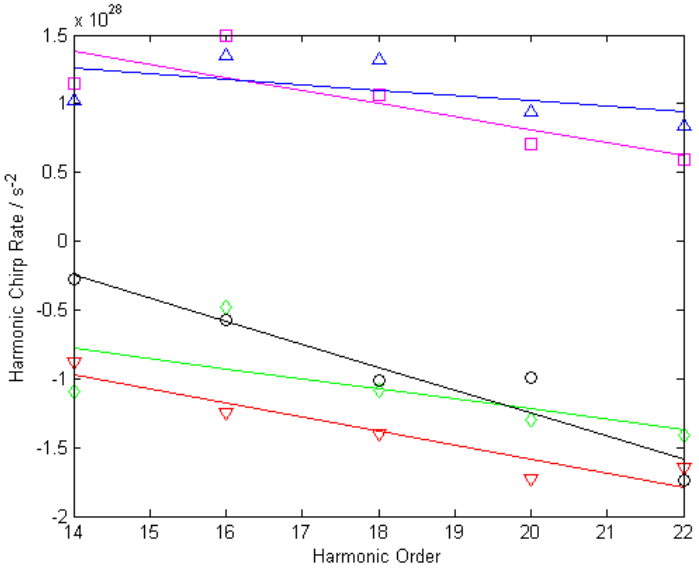

Figure 5.12: Harmonic chirp rate calculated by Mauritsson *et al.* plotted as a function of harmonic order. Red colour – case (a); green – (b); black – (c); (d) – purple; (e) – blue.

made in this project, using FROG traces from simple linearly chirped Gaussian pulses, show that the absolute value of b may be reduced by as much as 25% when threshold filtering. This is not enough to explain the whole reduction of the chirp rates, but it is large enough to be taken into account. Also, filtering high spatial frequencies in the XFROG trace too much has been found tho distort the retrieved phase, although in exactly what way the calculation of b is affected is hard to predict.

5.2 FROG CRAB Implementation

As stated in earlier chapters, not only single harmonic pulses may be characterized using PCGPA; it is also designed to make it possible to characterize attosecond pulses or even attosecond pulse trains, using FROG CRAB data. No modifications of the code is necessary – in the eyes of PCGPA all pulses are equal, as long as they come with a FROG trace. This section will focus on pulse retrieval using simulated FROG CRAB data, ending with a brief discussion regarding the difficulties and possibilities of pulse characterization using experimental data.

5.2.1 Implementation on Simulated Data

A simple way of designing a FROG trace with sidebands and sideband interference like those present in a RABITT scan, is by using an artificial and

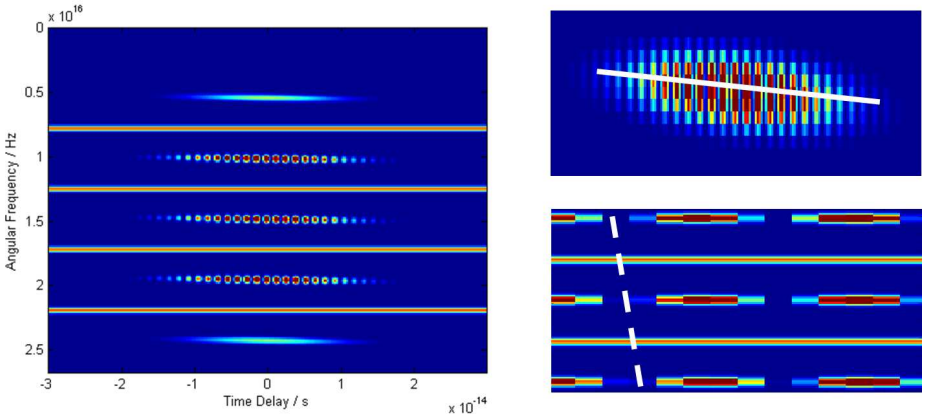

Figure 5.13: The the left: Attosecond pulse train made by harmonics 9-15. Up to the right: Tilt of sideband due to the harmonic chirp. Down to the right: Constructive respectively destructive interference changing from sideband to sideband, due to the atto chirp.

rather unphysical gate with the form of $1 + \Lambda(t) \cdot (e^{i\omega_0 t} + e^{-i\omega_0 t})$, where $\Lambda(t)$is an amplitude factor. The two exponentials lead to sidebands due to stimulated absorption and emission of one IR photon with the frequency ω_0. This trick makes the harmonics themselves appear in the FROG trace, since now $E(t) \cdot G(t) = E(t) + E(t)\Lambda(t) \cdot (e^{i\omega_0 t} + e^{-i\omega_0 t})$.

In figure 5.13, to the left, we show a simulated FROG CRAB scan using harmonics 9-15, exhibiting both harmonic and atto chirp. The 800 nm-gate pulse has an FWHM of 12 fs and is Fourier limited. In figure 5.14 the train itself is plotted, together with the temporal phase variation due to the harmonic chirp ($\partial^2\Phi/\partial t^2 \cdot t^2$) and the spectral phase variation due to the atto chirp ($\partial^2\Phi/\partial\omega^2 \cdot \omega^2$).

We start with trying to retrieve both pulse and gate from the FROG CRAB trace, using the PCGPA as a blind-FROG. The retrieved train is shown to the left in figure 5.15, and to the right, the FROG error as a function of the iteration number is plotted. Here one can see that the algorithm converges to a relatively low FROG error, but while the rough features of the train is retrieved, the train does not look like its original on a more detailed level. Also, it is found that the retrieved phases do not match the original at all. However, the initial guesses seem to affect the final blind-FROG result to a certain degree, which opens the possibility of improving the results by starting out with particulary good guesses. Such an optimisation has however not been carried out in this project.

When assuming the gate to be well-characterized, the result, shown in figure 5.16, is improved. The error is found to steady go down below 10^{-15} in 800 iterations, and one is able to both retrieve the envelope of the field, as well as the temporal and spectral chirps.

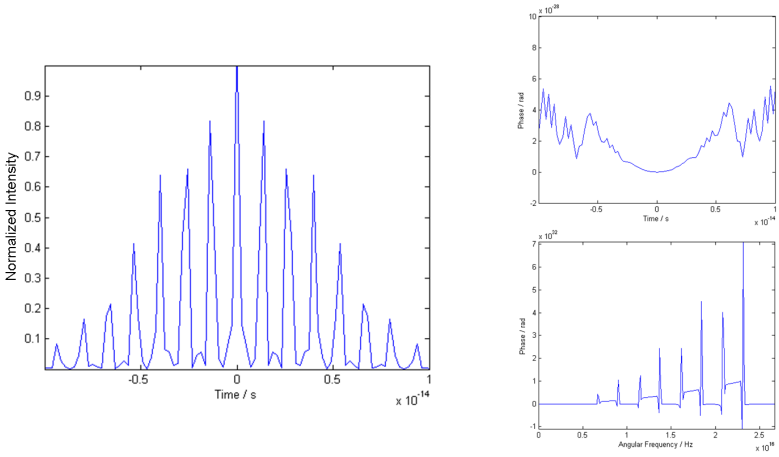

Figure 5.14: To the left: Attosecond pulse train constituted by harmonics 9-15. Up to the right: $\partial^2\Phi/\partial t^2 \cdot t^2$. Down to the right: $\partial^2\Phi/\partial q^2 \cdot \omega^2$

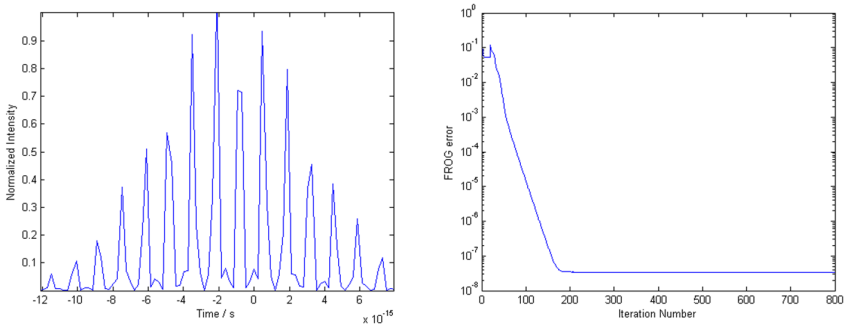

Figure 5.15: To the left: Retrieved attosecond pulse train using the blind-FROG algorithm. To the right: The FROG error for the blind-FROG iteration.

The FROG CRAB simulations have up until now been based on harmonics each carrying the same harmonic chirp. However this may not always be the case, which for instance can be seen in the graph in figure 5.11. Figure 5.17 depicts a pulse train and its corresponding FROG CRAB trace, with a harmonic chirp which is linearly dependent on q. The change of the chirp manifests itself quite intuitively in the FROG signal by a change of the tilt of the sidebands. This q-dependence will in the temporal domain give rise to a change of spacing between consecutive attosecond pulses in the train, as indicated in the figure. The pulse train, including the varying pulse to pulse spacing, is well retrieved using a forced gate as drawn in figure 5.18. The FROG error is converging to an error below 10^{-6} in 800 iterations.

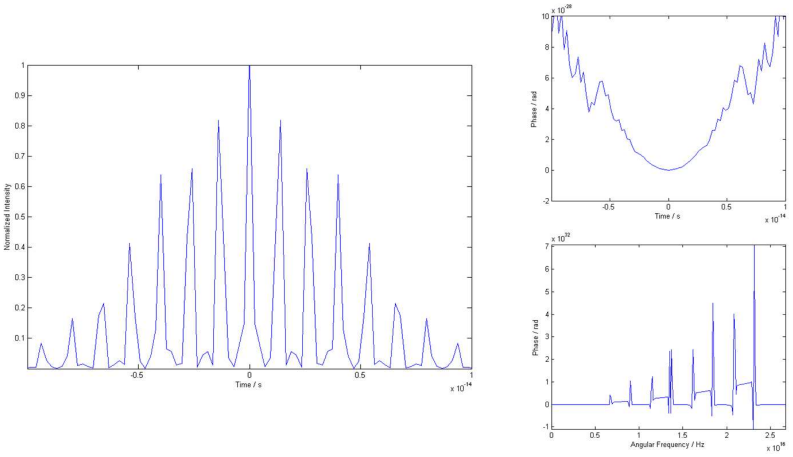

Figure 5.16: To the left: Retrieved pulse train from the FROG trace given in figure 5.13. To the right: At the top, retrieved temporal phase variation; at the bottom, retrieved spectral phase variation.

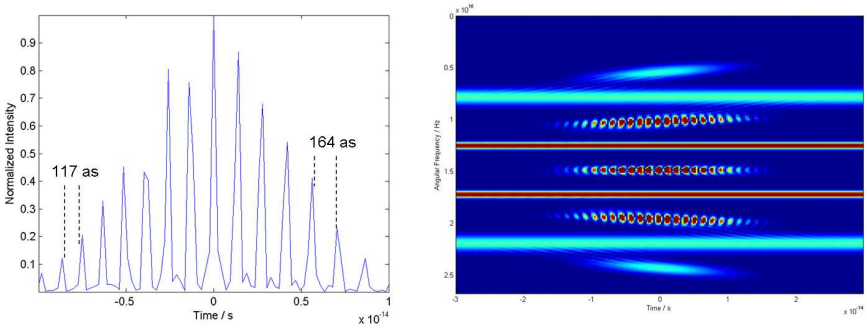

Figure 5.17: To the left: Pulse train with a q-dependence of the harmonic chirp, $b = b(q)$. The pulse separation is indicated in the figure. To the right: The FROG trace of the train.

5.2.2 Implementation on Experimental Data

While proposed [13] [17], implementing FROG CRAB on experimental data has to this date never been performed. From a computational point of view, there are at least two possible complications which can come up when attempting to retrieve a pulse train in the laboratory: First, the two outer sidebands in a FROG CRAB scan are often missing in experimental scans. This will introduce an error in the PCGPA calculations. Second, the resolution of the MBES device is worsened when the energy of the electrons is increased. This will lead to a frequency broadening of the high-order sidebands which may make the algorithm not to converge properly. A possible solution of this problem would be to do the whole scan segment-wise. When going higher up in energy, one would then apply a voltage in order slow the electrons down, and by this increase the resolution once again [24].

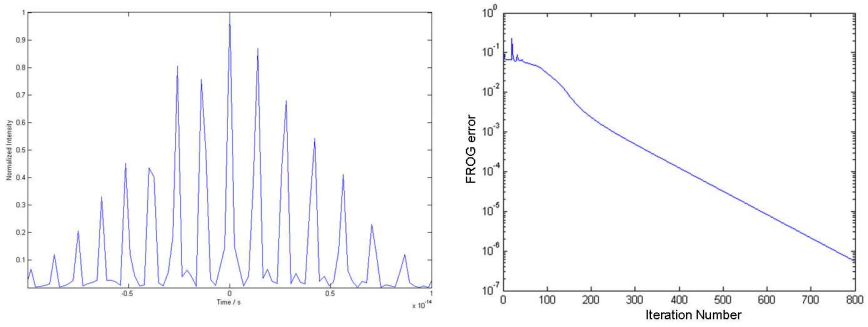

Figure 5.18: Attempting to characterize a pulse train where $b = b(q)$, using a forced gate. To the left: Retrieved pulse train. To the right: The FROG error.

Chapter 6

Summary and Concluding Remarks

The goal of this project was to write an algorithm based on the method of PCGP and to implement it on FROG data. Results from simultated FROG data has shown that the algorithm works sucessfully, even when used as a blind-FROG. However, if the pulse and the gate both are symmetric and quite similar in shape, there is a risk of a mix-up or 'average-value' pulses as a result of the retrieval procedure. The introduction of an additional constraint in the form of the spectrum of the unknown pulse has been found to increase the convergence rate – if correctly applied. If the gate pulse can be regarded as already being properly characterized, it is possible to 'force' this known gate in each iteration, which makes the algorithm more likely to converge.

When using experimental XFROG data, with sidebands as input, in order to characterize femtosecond high-order harmonics in the XUV domain, the blind-FROG does however not seem to work equally good. This problem can partially be overcome by characterizing the gate using some other method, and then assuming the gate to be known when performing the iterations. The calculations of the harmonic chirp rate has shown to give values which are about one third of what is to be expected, as well of what has been calculated using other procedures. The reason for this is still unknown. The treatment of the data before sending it into the algorithm, in order to filter it from noise, etc, may give a small error of the phase. Also, the spatial dependence of the pulses is completely neglected in the model which the algorithm is based on, which may give rise to errors of significant magnitude. Modifying the algorithm with respect to this might give better values; this has however not been done, considering the limited time range of this project.

Simulated attosecond pulse trains have also been retrieved using artificial FROG CRAB data. Both spectral and temporal second-order phase terms have been reproduced, using a forced gate function in the iteration. Even if the blind-FROG algorithm in this project did not fully succeed in retrieving both pulse

and gate at the same time, it has however been done, see for instance Mairesse *et al.* [13]. In order to improve and assure convergence one might for instance improve the initial guesses of the program, or find a more suitable way of applying the additional spectral constraint.

Up until this date, using the PCGPA for characterizing pulse trains experimentally has not been done. The good results from the simulations made in this project shows however that it is very likely that this can be done, given good experimental conditions. Today, in order to characterize an attosecond pulse train, one must combine several different measurement methods; for instance by XFROG one measures the harmonic chirp, and by RABITT one obtains the atto chirp. In the near future, however, one might just be able to extract all this information from a single scan, for instance in the form of a FROG CRAB trace.

Chapter 7

Acknowledgements

First I would like to thank my supervisor *Anne L'Huillier* for introducing me to the the field of ultrashort laser physics and giving me the opportunity to do my diploma project within the high-order harmonic generation research group. Her help has been vital for this project, and has manifested itself in a number of ways – by answering all of my questions and coming with valuable suggestions, as well as functioning as a source of general encouragement.

I would also like to thank the rest of the research group for all the help they have given me through this project: *Per Johnsson*, *Katalin Varjú* and *Erik Gustafsson*. Especially I would like to thank *Thomas Remetter* for the countless number of times he has taken his time to answer all of the questions I have harassed him with. Also, fellow diploma worker *Nils Adie* has been a refreshing companion during the time I have had the pleasure of sharing my office with him.

I also visited *Le Centre CEA de Saclay* for one day, where *Yann Mairesse* showed me around and discussed FROG CRAB with me; for this I am thankful.

In the end, I would like to thank my family, especially my mother, my father and my sister, who always have given me unlimited support during the years. After all, if it were not for the first two, I would not even be sitting here today, typing. And you just got to give them some cred for that, right?

Bibliography

[1] D.J. Kane, R. Trebino, IEEE J. Quantum Electron., **29**, 571, 1993

[2] J.C. Diels, W. Rudolph, *Ultrashort Laser Pulse Phenomena – Fundamentals, Techniques and Applications on a Femtosecond Time Scale*, Academic Press, 1996

[3] M.N.O. Sadiku, *Elements of Electromagnetics*, Oxford University Press, 2001

[4] P. Johnsson, *Adaptive Laser Pulse Shaping using an Acousto-Optic Programmable Dispersive Filter and a Genetic Algorithm*, Master's Thesis, Lund Reports on Atomic Physics, LRAP-291, 2002

[5] O. Svelto, *Principles of Lasers*, Plenum Press, 1998

[6] J. Mauritsson, *Temporal Aspects of High-Intensity Laser-Matter Interactions*, Doctoral Thesis, Lund Reports on Atomic Physics, LRAP-312, 2003

[7] L. Roos, *Optimisation and Application of Intense High-Order Harmonic Pulses*, Doctoral Thesis, Lund Reports on Atomic Physics, LRAP-276, 2001

[8] S. Häßler, M. Swoboda, *Optimisation and Application of High-Order Harmonics of an Ultrashort Terrawatt Laser*, Report, Lund Reports on Atomic Physics, LRAP-324, 2004

[9] K. Varjú, Y. Mairesse, B. Carré, M.B. Gaarde, P. Johnsson, S. Kazamias, R. López-Martens, J. Mauritsson, K.J. Schafer, P. Balcou, A. L'Huillier, P. Salières, J. Mod. Opt. **52**, 379, 2005

[10] R. López-Martens, K. Varjú, P. Johnsson, J. Mauritsson, Y. Mairesse, P. Salières, M.B. Gaarde, K.J. Schafer, A. Persson, S. Svanberg, C.-G. Wahlström, A. L'Huillier, Phys. Rev. Lett. **94**, 033001, 2005

[11] Y. Mairesse, A. de Bohan, L.J. Frasinski, H. Merdji, C. Dinu, P. Monchicourt, P. Berger, M. Kovačev, R. Taïeb, B. Carré, H.G. Muller, P. Agostini, P. Salières, Science **302**, 1540, 2003

[12] S. Linden, H. Giessen, J. Kuhl, Phys. Stat. Sol. B **206**, 119, 1998

[13] Y. Mairesse, F. Quéré, Phys. Rev. A **71**, 011401, 2005

[14] R. Trebino, K.W. DeLond, D.N. Fittinghoff, J.N. Sweetser, M.A. Krumbügel, B.A. Richman, D.J. Kane, Rev. Sci. Instrum. **68**, 3277, 1997

[15] J. Norin, J. Mauritsson, A. Johansson, M.K. Raarup, S. Buil, A. Persson, O Dühr, M.B. Gaarde, K.J. Schafer, U. Keller, C.-G. Wahlström, A. L'Huillier, Phys. Rev. Lett. **19**, 193901, 2002

[16] K. Varjú, P. Johnsson, R. López-Martens, T. Remetter, E. Gustafsson, A L'Huillier, J. Mauritsson, M.B. Gaarde, K.J. Schafer, C. Erny, I. Sola, A. Zaïr, E. Constant, E. Cormier, E. Mével, ???

[17] F. Quéré, Y. Mairesse, J. Itatani, J. Mod. Opt. **52**, 339, 2005

[18] D.J. Kane, G. Rodriquez, A.J. Taylor, T. Sharp Clement, J. Opt. Soc. Am. B **14**, 935, 1997

[19] K.W. DeLong, R. Trebino, J. Opt. Soc. Am. **11**, 2429, 1994

[20] K.W. DeLong, D.N. Fittinghoff, R. Trebino, B. Kohler, K. Wilson, Opt. Lett. **19**, 2152, 1994

[21] D.J. Kane, IEEE J. Select. Topics Quantum Electron. **4**, 278, 1998

[22] D.J. Kane, IEEE J. Quantum Electron. **35**, 421, 1999

[23] J. Mauritsson *et al.*, Phys. Rev. A **70**, 193901, 2004

[24] Discussions with Y. Mairesse.

Appendix A

The PCGP Algorithm

```
function [EGate,EPulse,e] = pulseRetrieval(IFrog,EGate,
    EPulse,ESpec,NbrIter)

% pulseRetrieval inverts the FROG trace using the power method.
% The input is the trace - IFrog - the initial two guesses -
% EGate and EPulse - a possible spectrum of the pulse - ESpec -
% and finally the number of iterations - NbrIter.
% The output are the two retrieved pulses, together with the FROG error
% function e.

% Defining the speed of light
c = 299792458;

% e = the FROG error
e = zeros(1,NbrIter);

% N = the number of elements of EPulse
N = length(EPulse);

% Esig = the FROG signal
Esig = zeros(N,N);

% The iteration loop starts
for k = 1:NbrIter

%The additional spectral constraint is applied
    if k == 20
        EPulseSpec = fft(EPulse);
        EPulseSpec = sqrt(ESpec).*EPulseSpec/(max(abs(EPulseSpec)));
        EPulse = ifft(EPulseSpec);
    end

% The outer product form matrix is created
```

```
    OP = EPulse.'*EGate;

% Row manipulation of OP
    for n = 2:N
        OP(n,:) = circshift(OP(n,:),[0,n-1]);
    end

% Column manipulation of OP; Esig in the time-time domain is created
    OP = fftshift(OP,2);
    Esig = fliplr(OP);

% Fourier transforming Esig columnwise; Esig is now i the time-frequency
% domain
    Esig = fft(Esig);

% Calculating the FROG error function e
    IFrogTemp = Esig.*conj(Esig);
    IFrogTemp = IFrogTemp/(max(max(abs(IFrogTemp))));

    IDiff = (IFrogExp-IFrog/(max(max(abs(IFrog))))).^2;
    e(k) = sqrt((sum(sum(IDiff)))/(N^2));

% Replacing the magnitude of Esig with experimental data
    Zero = abs(Esig) == 0;
    Esig = Esig + Zero;
    Esig = sqrt(IFrog).*(Esig./(abs(Esig)));

% Inverse Fourier transforming Esig back to the time-time domain
    Esig = ifft(Esig);

% Row and column manipulation Esig into its OP form
    Esig = fliplr(Esig);
    OP = fftshift(Esig,2);

    for n = 2: length(EInit)
        OP(n,:) = circshift(OP(n,:),[0,-(n-1)]);
    end

% Matrix-vector multiplication in order to obtain the next guesses
    EPulse = (OP*(OP')*EPulse.').';
    EPulse = EPulse/(max(abs(EPulse)));
    EGate = ((OP')*OP*EGate.').';
    EGate = EGate/(max(abs(EGate)));
end
```

Appendix B

The Chirp Rate Calculation Program

```
function [b] = chirpCalc(t,EPulse,start,stop)

% The function chirpCalc calculates the linear chirp rate of a pulse, b.
% The input is the time vector t, the pulse EPulse, and the area within one
% wants to polyfit the phase - start and stop.

N = length(t);
dt = t(2)-t(1);

% Calculates the argument of EPulse, and its derivative
arg = unwrap(angle(EPulse));
d_arg = unwrap(diff(arg));
d_arg = [d_arg(1) d_arg];

% Sets the limits in which the polyfit command should work
start = N/2+round(start/dt);
stop = N/2+round(stop/dt);

% Fits the data of the derivative of the argument as a first-degree
% polynomial, then extracts b
polyChirp = polyfit(t2(start:stop),d_arg(start:stop),1);
b = polyChirp(1)/dt
```